iScience

CellPress
OPEN ACCESS

Article

Tripartite motif 38 attenuates cardiac fibrosis after myocardial infarction by suppressing TAK1 activation via TAB2/3 degradation

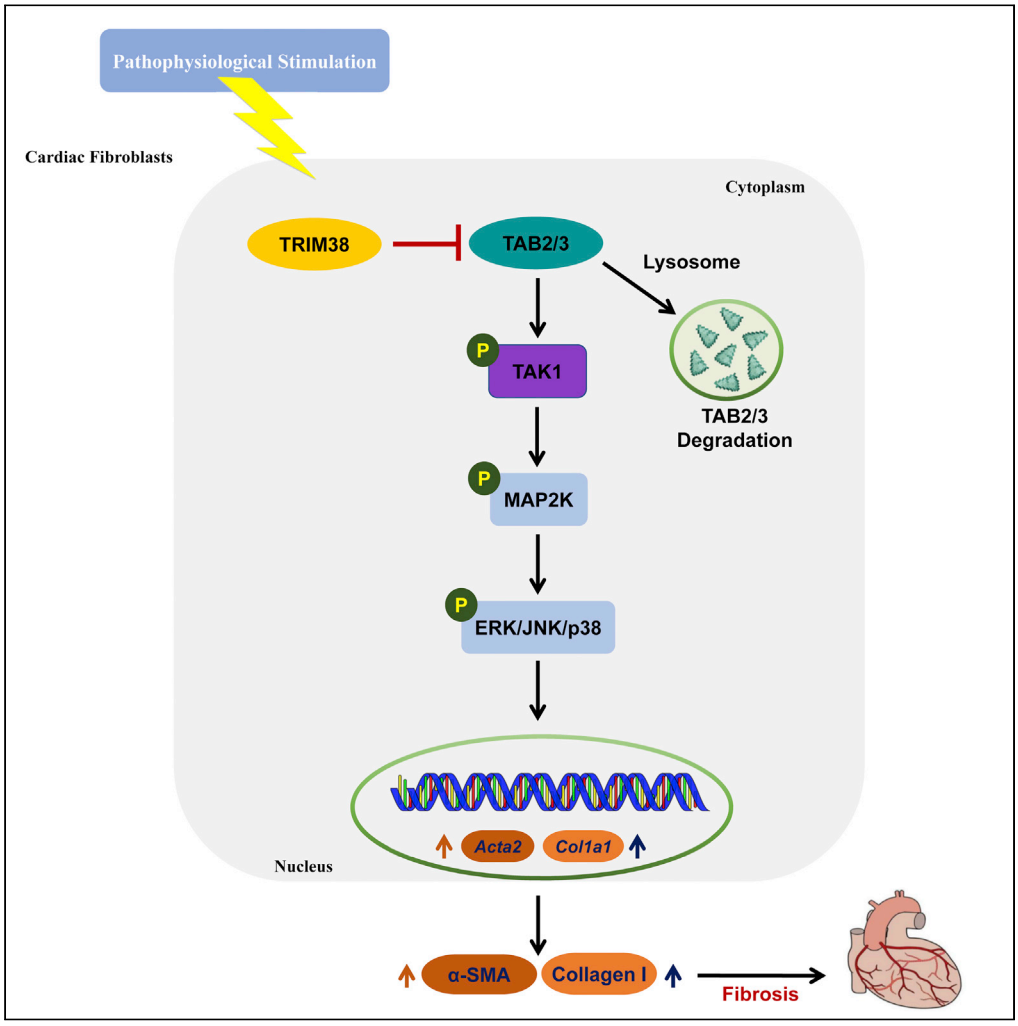

Zhengri Lu, Chunshu Hao, Hao Qian, ..., Yuyu Yao, Genshan Ma, Lijuan Chen

chenlijuan@seu.edu.cn

Highlights

TRIM38 expression is negatively correlated with cardiac fibrosis progression

TRIM38 ameliorates the proliferation and secretion of CFs post fibrotic stimulation

TRIM38 overexpression attenuates cardiac fibrosis progression in MI mice

TRIM38 inhibits the TAK1/MAPK pathway by targeting the degradation of TAB2 and TAB3

Lu et al., iScience 25, 104780
August 19, 2022
https://doi.org/10.1016/j.isci.2022.104780

iScience

CellPress
OPEN ACCESS

Article

Tripartite motif 38 attenuates cardiac fibrosis after myocardial infarction by suppressing TAK1 activation via TAB2/3 degradation

Zhengri Lu,[1] Chunshu Hao,[1] Hao Qian,[1] Yuanyuan Zhao,[1] Xiangwei Bo,[1] Yuyu Yao,[1] Genshan Ma,[1] and Lijuan Chen[1,2,3,*]

SUMMARY

The role of tripartite motif (TRIM) 38, a ubiquitin E3 ligase regulating various pathophysiological processes, in cardiac fibrosis remains unclear. Here, a model of angiotensin II and myocardial infarction (MI)-induced fibrosis was established to explore its role in cardiac fibrosis and its underlying mechanisms. Cardiac fibrosis in the mouse MI model was mitigated by TRIM38 overexpression, but aggravated by its depletion. Consistently, *in vitro* overexpression or knockdown of TRIM38 ameliorated or aggravated the proliferation and secretion of cardiac fibroblasts (CFs) exposed to fibrotic stimulation, respectively. Mechanistically, TRIM38 suppressed cardiac fibrosis progression by attenuating TAK1/MAPK signaling. Inhibiting TAK1/MAPK signaling with a pharmacological inhibitor greatly reversed the effects of TRIM38 knockdown on CF secretion. Specifically, TRIM38 interacted with and "targeted" TAB2 and TAB3 for degradation, subsequently inhibiting TAK1 phosphorylation and negatively regulating MAPK signaling. These findings can help develop therapeutic strategies to treat and prevent cardiac fibrosis.

INTRODUCTION

Acute myocardial infarction (AMI) is a serious cardiovascular disease that remains a leading cause of death worldwide. Percutaneous coronary intervention (PCI) significantly reduces mortality in patients with AMI. However, a considerable number of patients still experience excessive cardiac fibrosis or ventricular remodeling after infarction, which ultimately leads to cardiac insufficiency. Cardiac fibrosis is characterized by the deposition of extracellular matrix (ECM) proteins in the myocardium, and the initial "reparative fibrosis" is essential to suppress infarct expansion and prevent ventricular wall rupture. However, fine interstitial "reactive fibrosis" in non-ischemic myocardium after myocardial infarction (MI) appears to result from a distinct pathological process, leading to cardiac dysfunction and heart failure (Kong et al., 2014; Li et al., 2018). Cardiac fibroblasts (CFs) are the main cells in the heart that secrete ECM proteins and are key mediators of pathological cardiac remodeling (Frangogiannis, 2019). When subjected to ischemia, pressure, volume overload, or other pathological stimuli, CFs may migrate, proliferate, and differentiate into myofibroblasts, which phenotypically express α-smooth muscle actin (α-SMA), secrete large amounts of ECM proteins, and ultimately lead to decreased ventricular wall compliance and contractile dysfunction (Travers et al., 2016). Despite the pathophysiological importance of fibrosis in cardiovascular disease, there are no effective medical strategies to precisely intervene in these two types of fibrosis. Therefore, an in-depth understanding of the molecular mechanisms underlying cardiac fibrosis is crucial for the development of new anti-fibrosis strategies for the treatment of cardiac disease.

Many studies have indicated that the mitogen-activated protein kinase (MAPK) pathway plays a critical role in the initiation and progression of fibrosis (Ruperez et al., 2007; Tian et al., 2020). MAPK is a serine/threonine protein kinase that is highly conserved in eukaryotes and participates in a wide range of cellular activities including cell proliferation, differentiation, stress responses, apoptosis, and cell migration and survival (Frangogiannis, 2019). It also plays an indispensable role in cardiac signaling events (Frangogiannis, 2021; Tian et al., 2020). Although current studies have shown that persistent activation of the MAPK pathway is closely associated with the progression of cardiac fibrosis, there is still a lack of direct evidence for the role of the MAPK pathway in myocardial fibrosis *in vivo*, warranting further investigation.

[1]Department of Cardiology, Zhongda Hospital, Southeast University, Nanjing, China

[2]Department of Cardiology, Zhongda Hospital Lishui Branch, Southeast University, Nanjing, China

[3]Lead contact

*Correspondence: chenlijuan@seu.edu.cn

https://doi.org/10.1016/j.isci.2022.104780

Transforming growth factor β (TGF-β)-activated kinase 1 (TAK1, also known as MAP3K7) is a member of the mitogen-activated protein kinase kinase kinase (MAP3K) family and a downstream regulator of the TGF-β signaling pathway (Ajibade et al., 2013; Akira, 2003). TAK1 forms ternal complexes with the activator MAP3K7-binding proteins (TAB) (Ishitani et al., 2003; Shibuya et al., 1996). Among these proteins, TAB2 and TAB3 are essential for sustained TAK1 activation (Xu and Lei, 2020). These contain carboxy-terminal Npl4 zinc finger (NZF) domains that interact with polyubiquitin chains to promote TAK1 activation and trigger the downstream MAPK signaling pathway. Therefore, ubiquitination is critical for the activation of TAK1 (Kawai and Akira, 2006; Xu and Lei, 2020).

Tripartite motif (TRIM) proteins, a subfamily of the RING-type E3 ubiquitin ligase family, are characterized by the presence of an N-terminal RING finger domain, one or two B-box domains, and an associated coiled-coil domain (Hatakeyama, 2017; McNab et al., 2011). E3 ubiquitin ligase is responsible for substrate recognition and the specificity of ubiquitination, and regulates the quantity and functional activity of intracellular substrates. The TRIM family proteins are implicated in a broad range of cellular processes, including cell cycle regulation, transcriptional regulation, protein quality control, immune defense, and inflammatory responses (Hatakeyama, 2017; McNab et al., 2011). In addition, TRIM proteins have been shown to participate in the generation and development of multiple cardiovascular diseases, including arrhythmia, diabetic cardiomyopathy, ischaemic heart disease, and cardiac hypertrophy (Borlepawar et al., 2017; Guo et al., 2018; Liu et al., 2015a, 2015b, 2019b). We previously showed that TRIM8 and TRIM32 are involved in pathological cardiac remodeling (Chen et al., 2016, 2017). The E3 ubiquitin ligase TRIM38 is a typical member of the TRIM protein family (Hu et al., 2014; Liu et al., 2011). Owing to its RING finger domain, TRIM38 is thought to have E3 ubiquitin ligase activity. A large-scale human genome survey showed that TRIM38 has the ability to activate the nuclear factor-κB (NF-κB) and MAPK signaling pathways (Matsuda et al., 2003). Hu et al. (2014) used the HEK293T cell line and TRIM38 expression plasmid and found that TRIM38 can form a structural complex with TAB2/3 by virtue of its own carboxy-terminal PRY-SPRY domain, promote lysosomal degradation of TAB2/3, and negatively regulate IL-1 and TNF-α-induced TAK1 activation. These findings indicate that TRIM38 is an essential regulator of TAK1/MAPK signaling. Therefore, functional identification of TRIM38 might help to understand the pathological mechanism of cardiac fibrosis and explore the potential of TRIM38 as a therapeutic target for cardiac fibrosis following MI.

Here, we demonstrate that TRIM38 overexpression attenuates myocardial fibrosis, whereas its deficiency results in the opposite effect. Our evidence suggests that TRIM38 interacts with the TAK1-TAB2/3 complex in CFs. Through this interaction, TRIM38 "targeted" TAB2/3 for degradation and inhibited TAK1 phosphorylation, thus negatively regulating the activation of TAK1/MAPK kinases to exert anti-cardiac fibrosis effects. Collectively, our results indicate that TRIM38 is a novel negative regulator of pathological cardiac fibrosis and that its function is mainly to promote the degradation of TAB2/3 and inhibit the TAK1/MAPK signaling pathway.

RESULTS

TRIM38 expression is decreased in a mouse model of myocardial infarction

Expression of TRIM38 protein in paired coronary blood samples from patients with AMI (n = 5) and normal samples (n = 5) was evaluated using ELISA (basal clinical characteristics are presented in Tables S1 and S2). The serum level of TRIM38 was significantly lower in the AMI group than in paired normal controls (Figure S1A). MI-induced mouse myocardial fibrosis model was used to analyze the expression of TRIM38 in the fibrotic response *in vivo*. Cardiac function was measured using echocardiography four weeks post-MI. Echocardiography showed significantly decreased left ventricular fractional shortening (LVFS) and left ventricular ejection fraction (LVEF), while left ventricular internal dimension in diastole (LVIDd) and left ventricular internal dimension in systole (LVIDs) were significantly elevated in MI mice compared to those in sham mice (Figure 1A). To assess the extent of myocardial fibrosis after MI, the expression levels of collagen I and α-SMA, key markers of the fibrotic process, were analyzed and Masson's trichrome staining and immunohistochemistry were performed. Quantitation results revealed marked collagen deposition in MI mice compared to that in sham mice (Figure 1B). The expression of *Col1α1* and the fibrosis-related gene *Acta2* was significantly increased in MI mice (Figure S1B). Meanwhile, Western blotting results from MI mouse hearts demonstrated marked increases in the expression of the fibrosis markers collagen I and α-SMA (Figure 1C). However, TRIM38 expression was significantly reduced in the myocardia of MI mice compared with that in control mice (Figure 1C).

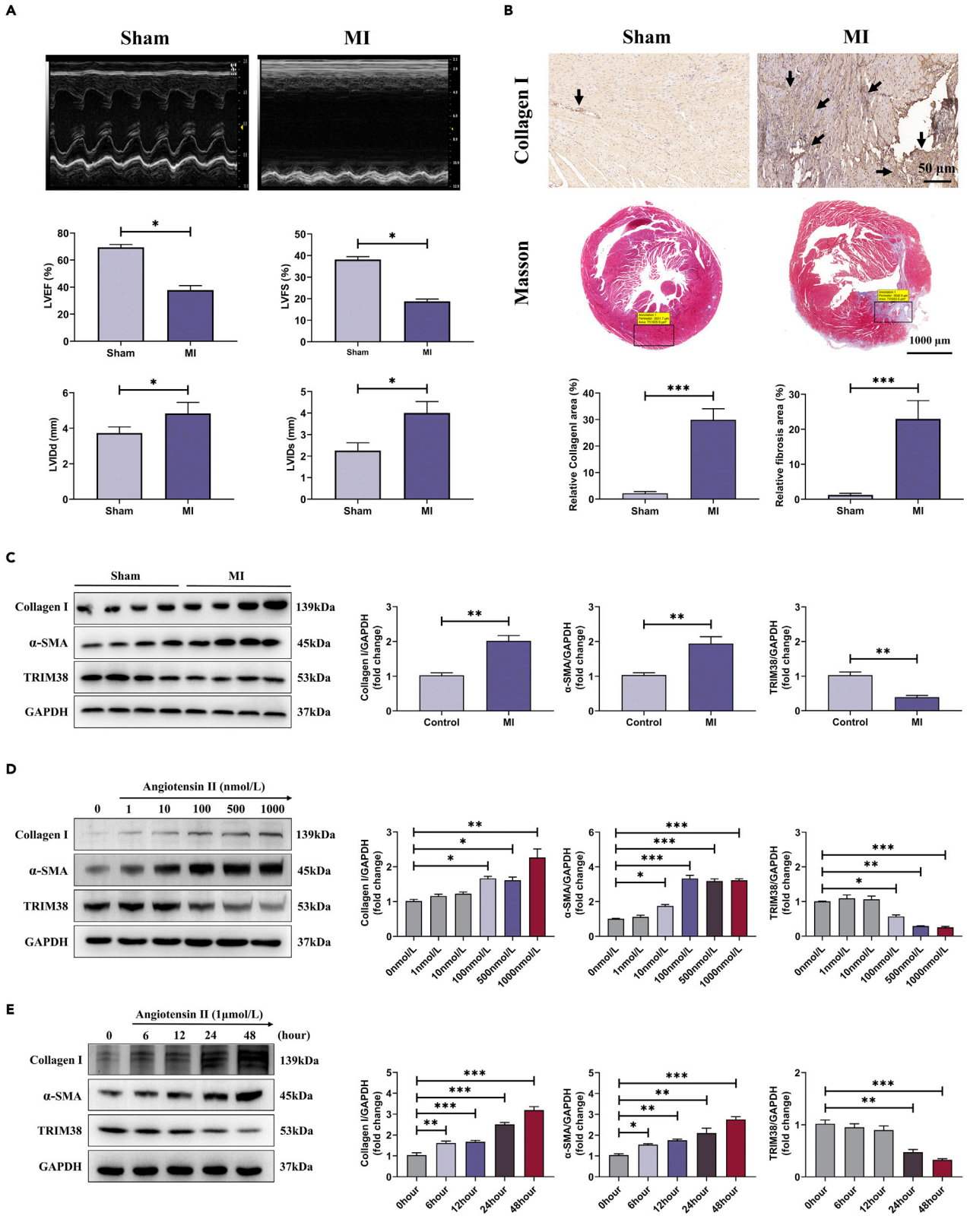
A
Sham
MI
LVEF (%)
LVFS (%)
LVIDd (mm)
LVIDs (mm)
B
Collagen I
Masson
50 μm
1000 μm
Relative CollagenI area (%)
Relative fibrosis area (%)
C
Collagen I
α-SMA
TRIM38
GAPDH
139kDa
45kDa
53kDa
37kDa
Collagen I/GAPDH (fold change)
α-SMA/GAPDH (fold change)
TRIM38/GAPDH (fold change)
Control
MI
D
Angiotensin II (nmol/L)
0
1
10
100
500
1000
0nmol/L
1nmol/L
10nmol/L
100nmol/L
500nmol/L
1000nmol/L
E
Angiotensin II (1μmol/L)
0
6
12
24
48
(hour)
0hour
6hour
12hour
24hour
48hour

Figure 1. Decreased expression of TRIM38 in the mice with myocardial infarction

(A) Representative M-mode echocardiographic images of each group. Echocardiographic analysis of cardiac function in mice at 28 days after MI or sham operation. LVEF: left ventricular ejection fraction; LVFS: left ventricular fraction shortening; LVIDd: left ventricular internal diameter in diastole; LVIDs: left ventricular internal diameter in systole. n = 4/each group; *p < 0.05, compared with Sham group.

(B) Representative images of immunohistochemical-stained (scale bar = 50 μm) and Masson's trichome-stained (scale bar = 1000 μm) myocardial sections at 28 days from MI or sham mice. Scar tissue and viable myocardium are identified in blue and red, respectively. The bar chart quantifies the collagen I content and the extent of fibrosis in each group.

(C) Representative Western blotting (Left) and quantitative results (Right) of collagen I, α-SMA, and TRIM38 protein expression in mice hearts induced by MI or sham operation for 28 days n = 4/each group; *p < 0.05, compared with Sham group.

(D) Representative Western blotting (Left) and quantitative results (Right) of collagen I, α-SMA, and TRIM38 protein expression in cultured neonatal rat cardiac fibroblasts (NRCFs) treated with angiotensin II for 48 h. Three independent experiments; *p < 0.05; **p < 0.01, compared with 0 nmol/L group.

(E) Representative Western blotting (Left) and quantitative results (Right) of collagen I, α-SMA, and TRIM38 protein expression in cultured NRCFs treated with angiotensin II (1 μmol/L) for 0, 6, 12, 24, and 48 h. Three independent experiments; *p < 0.05; **p < 0.01, compared with 0 h group. The result was means ± S.D., which was analyzed by unpaired Student t-test.

To explore the impact of TRIM38 on cardiac fibrosis *in vitro*, CFs isolated from neonatal rats were treated with angiotensin II, a commonly used stimulant for inducing the transformation of CFs (Schnee and Hsueh, 2000). CFs were identified by immunofluorescent staining for vimentin and S100A4 (Figure S1C). Western blot analysis showed that, compared with that in the PBS group, the expression of collagen I and α-SMA in CFs of the angiotensin II-treated group gradually increased, while that of TRIM38 decreased in a concentration-dependent manner and reached its lowest point at 1 μmol/L angiotensin II (Figure 1D). TRIM38 expression was markedly decreased in CFs after stimulation with angiotensin II for 48 h (Figure 1E). Taken together, these data suggest that TRIM38 deficiency correlates with the development of cardiac fibrosis.

TRIM38 inhibits the transformation of cardiac fibroblasts to myofibroblasts *in vitro*

Owing to the decreased expression of TRIM38 during the development of cardiac fibrosis, we investigated whether TRIM38 could regulate disease progression. Recombinant adenoviruses for TRIM38 were constructed, and their knockdown and overexpression efficiencies were verified. Knockdown and overexpression of TRIM38 were confirmed by Western blotting (Figures 2A and 2B). CFs were then treated with either angiotensin II (1 μmol/L) or PBS for 48 h before measuring the expression levels of collagen I and α-SMA. The protein expression levels of collagen I and α-SMA were not significantly different between the PBS-treated groups. TRIM38 knockdown promoted the conversion of angiotensin II-induced CFs to myofibroblasts, as indicated by the increased expression of collagen I and α-SMA (Figure 2C). Immunofluorescence staining and real-time PCR showed similar results (Figures 2E and S2A). Moreover, wound-healing assays revealed that TRIM38 knockdown promoted angiotensin II-induced CF migration (Figure 2G). Conversely, we overexpressed TRIM38 in CFs by infecting with AdTRIM38 (Figures 2A and 2B), followed by a 48 h treatment with angiotensin II or PBS, as a control. TRIM38 overexpression significantly reduced the expression of collagen I and α-SMA stimulated by angiotensin II in CFs (Figure 2D). Immunofluorescence staining and real-time PCR showed consistent results (Figures 2F and S2B). Additionally, TRIM38 overexpression repressed angiotensin II-induced CF migration (Figure 2H). These *in vitro* data suggest that TRIM38 may act as a negative regulator of CF activation.

TRIM38 deficiency aggravates myocardial infarction-induced cardiac fibrosis

To investigate whether knockdown of TRIM38 would worsen MI-induced cardiac fibrosis *in vivo*, we intramyocardially injected adeno-associated virus 9 (AAV9)-shRNA-TRIM38 into mice to knock down TRIM38. AAV9-shRNA-NC cells were used as a control. The study design schedule is shown in Figure 3A. TRIM38 knockdown was confirmed by Western blotting (Figure S3). Two weeks after the injection, the mice were subjected to either MI or sham procedures. Cardiac function was analyzed using echocardiography at 4 and 28 days after the operation. AAV9-shRNA-TRIM38 mice had no apparent abnormalities in cardiac morphology or function compared with AAV9-shRNA-NC mice 28 days after sham operation (Figures 3B and 3C). MI induced a decrease in cardiac function in AAV9-shRNA-NC mice, and this induction was more significant in the hearts of AAV9-shRNA-TRIM38 mice (Figures 3B and 3C). Next, we stained cardiac sections with hematoxylin and eosin (HE) and Masson's staining to further evaluate the extent of myocardial disorder and fibrosis. At 28 days after MI, AAV9-shRNA-TRIM38 mice exhibited more prominent myocardial disorder and cardiac interstitial fibrosis than AAV9-shRNA-NC mice (Figures 3D and 3E). Meanwhile, immunohistochemical staining showed that collagen deposition increased in AAV9-shRNA-TRIM38 mice compared with that in AAV9-shRNA-NC mice (Figures 3D and 3E). Moreover, compared to AAV9-shRNA-NC mice, the elevated mRNA expression levels of the cardiac fibrosis markers *Col1α1* and *Acta2*

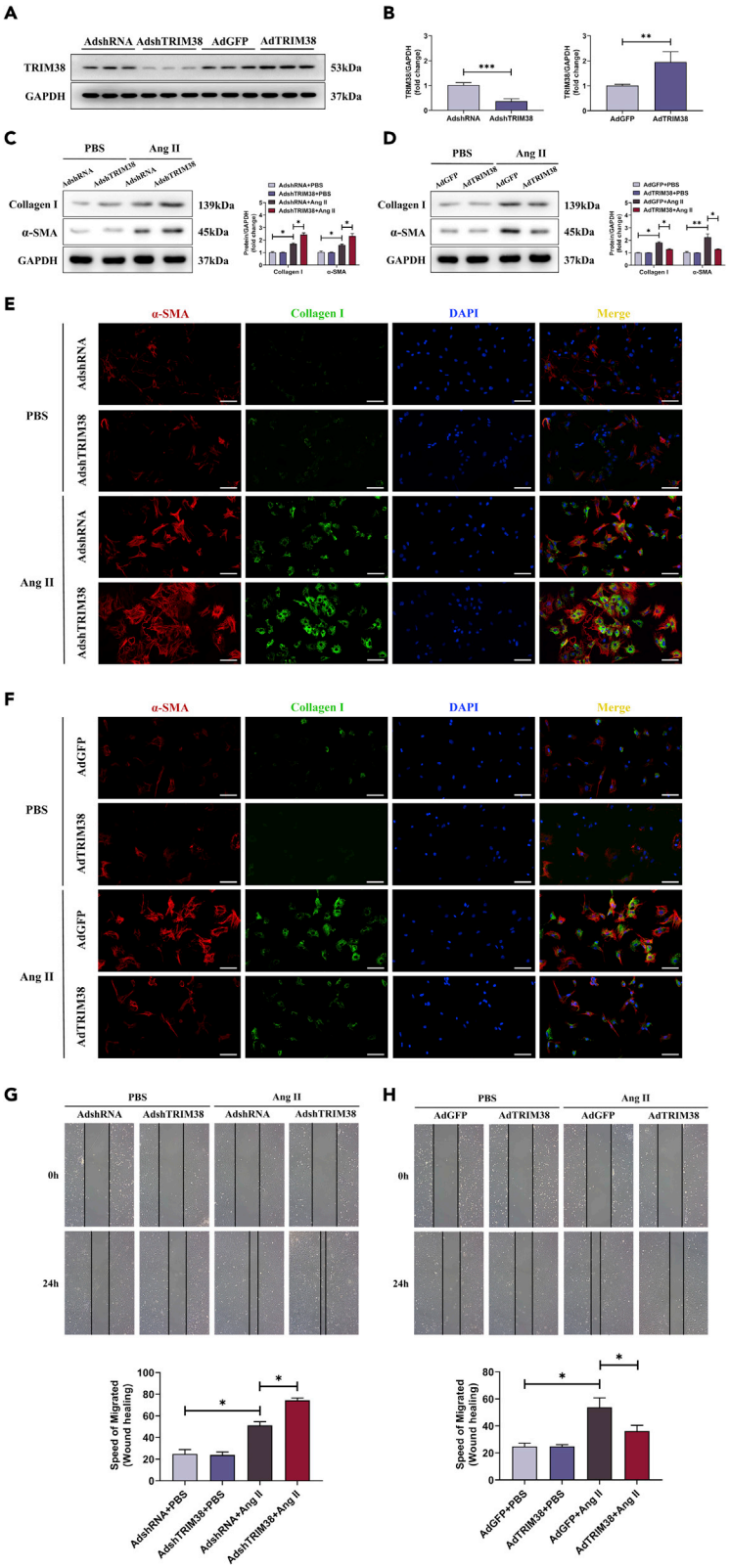
A
AdshRNA AdshTRIM38 AdGFP AdTRIM38
TRIM38
GAPDH
53kDa
37kDa
B
TRIM38/GAPDH (fold change)
***
AdshRNA AdshTRIM38
**
AdGFP AdTRIM38
C
PBS
Ang II
AdshRNA AdshTRIM38 AdshRNA AdshTRIM38
Collagen I
α-SMA
GAPDH
139kDa
45kDa
37kDa
AdshRNA+PBS
AdshTRIM38+PBS
AdshRNA+Ang II
AdshTRIM38+Ang II
Protein/GAPDH (fold change)
Collagen I
α-SMA
D
PBS
Ang II
AdGFP AdTRIM38 AdGFP AdTRIM38
Collagen I
α-SMA
GAPDH
139kDa
45kDa
37kDa
AdGFP+PBS
AdTRIM38+PBS
AdGFP+Ang II
AdTRIM38+Ang II
Collagen I
α-SMA
E
α-SMA
Collagen I
DAPI
Merge
PBS
Ang II
AdshRNA
AdshTRIM38
F
α-SMA
Collagen I
DAPI
Merge
PBS
Ang II
AdGFP
AdTRIM38
G
PBS
Ang II
AdshRNA AdshTRIM38 AdshRNA AdshTRIM38
0h
24h
Speed of Migrated (Wound healing)
AdshRNA+PBS
AdshTRIM38+PBS
AdshRNA+Ang II
AdshTRIM38+Ang II
H
PBS
Ang II
AdGFP AdTRIM38 AdGFP AdTRIM38
0h
24h
Speed of Migrated (Wound healing)
AdGFP+PBS
AdTRIM38+PBS
AdGFP+Ang II
AdTRIM38+Ang II

Figure 2. TRIM38 inhibits the transformation of cardiac fibroblasts to myofibroblasts *in vitro*

(A and B) Representative Western blotting (Left) and quantitative results (Right) of TRIM38 protein expression in NRCFs transfected with AdshTRIM38 or AdTRIM38. Three independent experiments; *p < 0.05.

(C and D) Representative Western blotting (Left) and quantitative results (Right) of collagen I and α-SMA protein expression in NRCFs transfected with AdshTRIM38 or AdTRIM38 stimulated with angiotensin II. Three independent experiments; *p < 0.05; **p < 0.01.

(E and F) Representative immunofluorescence staining image of collagen I and α-SMA in NRCFs stimulated with angiotensin II or not. NRCFs transfected with AdshTRIM38 or AdTRIM38. Scale bar = 50 μm.

(G and H) Migration ability of transfected with AdshTRIM38 or AdTRIM38 derived from indicated NRCFs detected by wound healing assay. Three independent experiments; *p < 0.05. The result was means ± S.D. Statistics in A and B was performed using unpaired Student t-test. Statistics in C, D and G, H were performed using a one-way ANOVA.

confirmed the aggravation of cardiac fibrosis in AAV9-shRNA-TRIM38 mice (Figure 3F). Altogether, TRIM38 knockdown did not lead to pathological alterations in the sham-operated group but significantly increased the susceptibility of the heart to cardiac fibrosis induced by MI.

TRIM38 overexpression attenuates myocardial infarction-induced cardiac fibrosis

AAV9-TRIM38 was intramyocardially injected into mice to compensate for TRIM38 overexpression and to further explore the effect of increased TRIM38 on cardiac fibrosis *in vivo* (Figure S4). Two weeks after the injection, AAV9-TRIM38 and AAV9-NC mice underwent MI or sham surgery (Figure 4A). At 4 and 28 days after MI, all mice were subjected to echocardiography to measure the cardiac parameters. TRIM38 overexpression improved cardiac function and inhibited MI-mediated myocardial fibrosis. Echocardiographic analysis showed significant improvement in LVEF and LVFS and a decrease in the left ventricular diameter in AAV9-TRIM38 mice compared with that in AAV9-NC mice at 28 days after MI (Figures 4B and 4C). In addition, HE and Masson's staining was used to evaluate the extent of myocardial disorder and fibrosis. Myocardial disorders and cardiac interstitial fibrosis were markedly alleviated in AAV9-TRIM38 mice after MI (Figures 4D and 4E). Similarly, immunohistochemical staining showed that collagen deposition decreased in AAV9-TRIM38 mice compared to that in AAV9-NC mice (Figures 4D and 4E). Accordingly, the mRNA expression levels of *Col1α1* and *Acta2* were markedly increased in AAV9-NC mice but were attenuated in AAV9-TRIM38 mice after MI (Figure 4F). Collectively, TRIM38 overexpression ameliorated cardiac fibrosis and improved cardiac function *in vivo* after MI.

TRIM38 inactivates TAK1/MAPKs signaling during myocardial infarction

To clarify the mechanism by which TRIM38 plays a cardioprotective role in cardiac fibrosis, we next investigated the state of MAPK signaling pathways, which are known to be involved in pathological cardiac fibrosis. c-Jun N-terminal kinase (JNK), extracellular signal-regulated kinase 1/2 (ERK1/2), and p38 MAPK, key mediators of the MAPK cascade, have been reported to be involved in various fibrotic diseases (Frangogiannis, 2021; van Berlo et al., 2013). MI-induced phosphorylation of p38, ERK1/2, and JNK1/2 was significantly enhanced in AAV9-shRNA-TRIM38 mice but attenuated in AAV9-TRIM38 mice (Figures 5A and 5B). However, the total expression of p38, ERK1/2, and JNK1/2 was not altered in the tested groups (Figures 5A and 5B).

Consistent with the *in vivo* results, TRIM38 knockdown enhanced the phosphorylation of p38, ERK1/2, and JNK1/2 in angiotensin II-induced CFs. In contrast, TRIM38 overexpression inhibited the phosphorylation of p38, ERK1/2, and JNK1/2 (Figures 5C and 5D). TAK1 is an upstream signaling molecule of MAPK (Bansal et al., 2017), is involved in pathological myocardial fibrosis (Koitabashi et al., 2011; Zhang et al., 2000), and has been confirmed to be regulated by TRIM38. We investigated whether TRIM38 regulates TAK1 signaling during MI. As expected, TAK1 baseline phosphorylation levels were not affected by changes in TRIM38 expression. MI-induced phosphorylation of TAK1 was significantly increased in AAV9-shRNA-TRIM38 mice but markedly ameliorated in AAV9-TRIM38 mice (Figures 5A and 5B). *In vitro* experiments with TRIM38 knockdown and overexpression further corroborated these results (Figures 5C and 5D). These findings indicate that TRIM38 mediates cardiac fibrosis by inhibiting the TAK1/MAPK signaling pathways.

Blocking TAK1/MAPK signaling rescues the angiotensin II-induced transformation of cardiac fibroblasts to myofibroblasts

To confirm the hypothesis that TRIM38 exerts cardioprotective effects by inhibiting the TAK1-dependent signaling pathway, we used the TAK1-specific inhibitor 5Z-7-oxozeaenol in rescue experiments. We aimed to determine if 5Z-7-oxozeaenol could inhibit TRIM38 knockdown-induced CF activation by

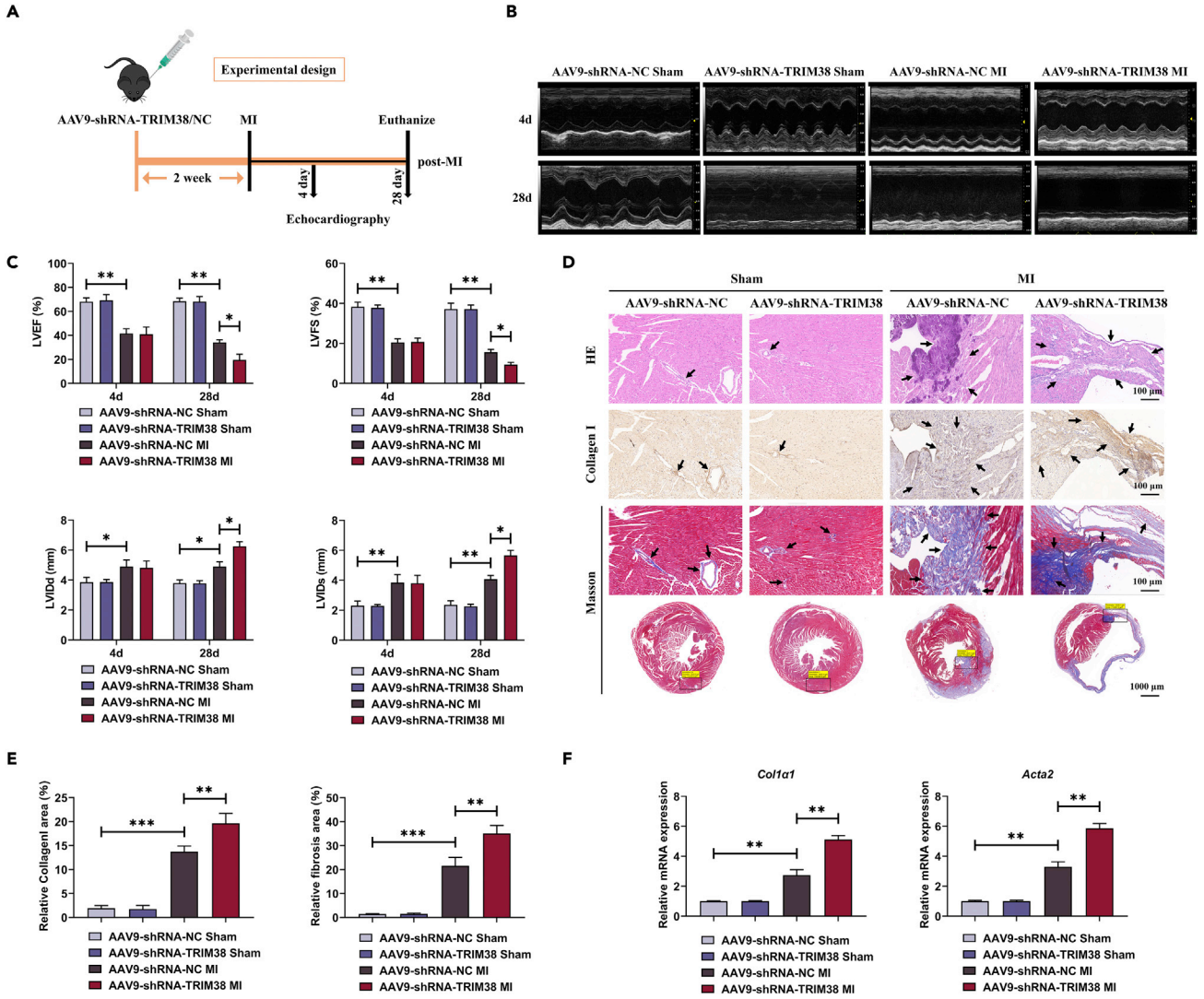

Figure 3. TRIM38 deficiency aggravates MI-induced cardiac fibrosis

Male C57BL/6 mice aged 8 weeks were subjected to MI or sham operation.

(A) Schematic of the experimental procedure.

(B and C) Representative and quantitative analysis of cardiac functions at 4 weeks post-MI. Echocardiographic parameters: LVEF; LVFS; LVIDd; LVIDs. n = 4–6/each group; *p < 0.05, **p < 0.01.

(D) Representative images of hematoxylin and eosin (H&E) staining, immunohistochemistry (IHC) staining of collagen I, and Masson's trichrome-stained in myocardium of mouse hearts after sham or MI operation. The lower scale bar indicates 100 μm and higher scale bar indicates 1000 μm.

(E) Quantitative analysis of Masson's trichrome-stained and collagen content between the groups. n = 4–6/each group; **p < 0.01, ***p < 0.001.

(F) Relative mRNA levels of *Col1α1* and *Acta2* in each group were determined by real-time PCR assays. n = 4–6/each group; **p < 0.01. The result was means ± S.D., and statistical analyses were performed using one-way ANOVA.

blocking TAK1-dependent signaling. Western blot analysis showed that 5Z-7-oxozeaenol reduced TAK1 phosphorylation in angiotensin II-treated CFs (Figures 6A and 6B). TRIM38 knockdown resulted in angiotensin II-induced upregulation of TAK1-dependent signaling component phosphorylation (Figures 6C and 6D). Moreover, compared to DMSO-treated controls, the increase in TAK1-dependent signaling component phosphorylation following TRIM38 knockdown was markedly alleviated by 5Z-7-oxozeaenol treatment (Figures 6C and 6D). Furthermore, 5Z-7-oxozeaenol reversed TRIM38 knockdown-induced conversion of CFs to myofibroblasts. Immunofluorescence staining (Figure 6E) and Western blotting (Figures 6F and 6G) showed that the inhibition of TAK1/MAPK signaling blocked the pro-fibrotic effects of TRIM38 knockdown in angiotensin II-stimulated CFs. This was confirmed by decreased protein

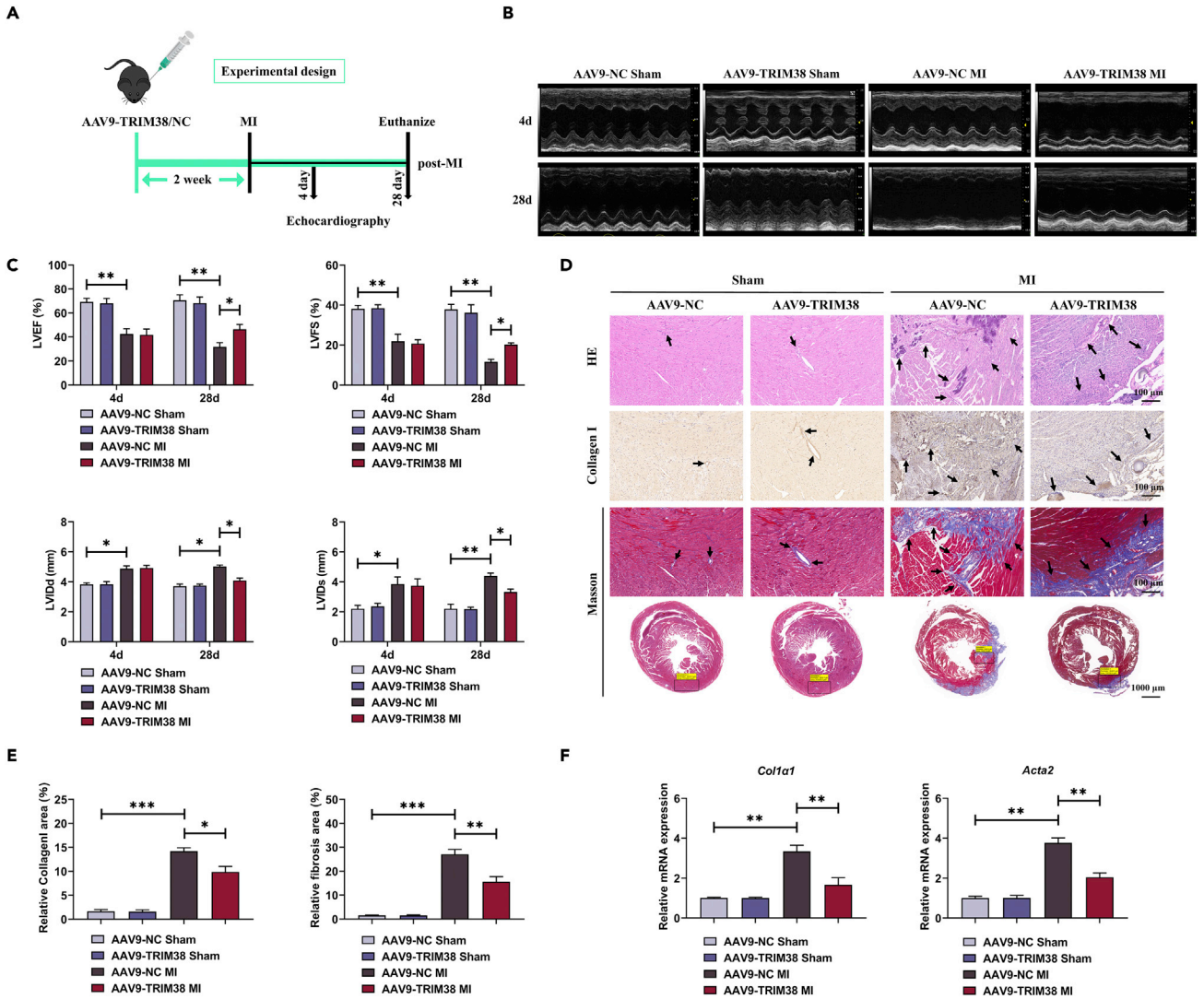

Figure 4. TRIM38 overexpression attenuates MI-induced cardiac fibrosis

Male C57BL/6 mice aged 8 weeks were subjected to MI or sham operation.

(A) Schematic of the experimental procedure.

(B and C) Representative and quantitative analysis of cardiac functions at 4 weeks post-MI. Echocardiographic parameters: LVEF; LVFS; LVIDd; LVIDs. n = 4–6/each group; *p < 0.05, **p < 0.01.

(D) Representative images of hematoxylin and eosin (H&E) staining, immunohistochemistry (IHC) staining of collagen I and Masson's trichrome-stained in myocardium of mouse hearts after sham or MI operation. The lower scale bar indicates 100 μm and higher scale bar indicates 1000 μm.

(E) Quantitative analysis of Masson's trichrome-stained and collagen content between the groups. n = 4–6/each group; **p < 0.01, ***p < 0.001.

(F) Relative mRNA levels of *Col1α1* and *Acta2* in each group were determined by real-time PCR assays. n = 4–6/each group; **p < 0.01. The result was means ± S.D., and statistical analyses were performed using one-way ANOVA.

expression of collagen I and α-SMA. These data further validate that TRIM38 plays an anti-fibrotic role, mainly by inhibiting the activation of TAK1-dependent signaling pathways.

TRIM38 suppresses TAK1 activity by mediating TAB2/3 degradation

The TRIM38 protein functions as an E3 ubiquitin ligase to poly-ubiquitinate a target protein for its degradation or post-translational modification through the autophagy-lysosome and ubiquitin-proteasome pathways (Hu et al., 2015). Furthermore, k48-and k63-linked polyubiquitination are both necessary and sufficient to activate TAK1. Therefore, we tested whether TRIM38 promotes the polyubiquitination of TAK1. CFs were either unstimulated or stimulated with angiotensin II. Whole-cell lysates were

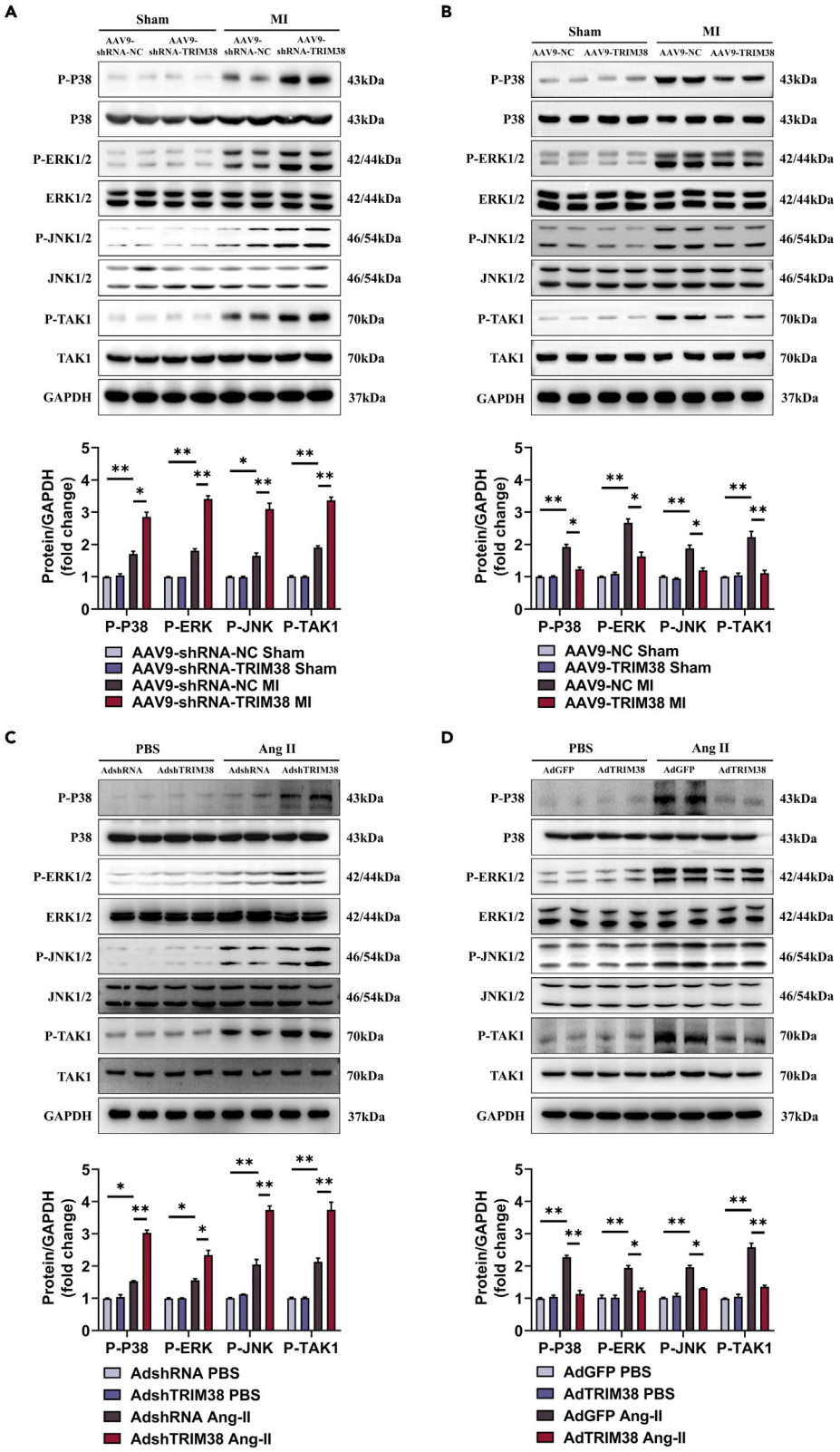
A
Sham
MI
AAV9-shRNA-NC
AAV9-shRNA-TRIM38
AAV9-shRNA-NC
AAV9-shRNA-TRIM38
P-P38
P38
P-ERK1/2
ERK1/2
P-JNK1/2
JNK1/2
P-TAK1
TAK1
GAPDH
43kDa
43kDa
42/44kDa
42/44kDa
46/54kDa
46/54kDa
70kDa
70kDa
37kDa
Protein/GAPDH (fold change)
P-P38
P-ERK
P-JNK
P-TAK1
AAV9-shRNA-NC Sham
AAV9-shRNA-TRIM38 Sham
AAV9-shRNA-NC MI
AAV9-shRNA-TRIM38 MI
B
Sham
MI
AAV9-NC
AAV9-TRIM38
AAV9-NC
AAV9-TRIM38
P-P38
P38
P-ERK1/2
ERK1/2
P-JNK1/2
JNK1/2
P-TAK1
TAK1
GAPDH
43kDa
43kDa
42/44kDa
42/44kDa
46/54kDa
46/54kDa
70kDa
70kDa
37kDa
Protein/GAPDH (fold change)
P-P38
P-ERK
P-JNK
P-TAK1
AAV9-NC Sham
AAV9-TRIM38 Sham
AAV9-NC MI
AAV9-TRIM38 MI
C
PBS
Ang II
AdshRNA
AdshTRIM38
AdshRNA
AdshTRIM38
P-P38
P38
P-ERK1/2
ERK1/2
P-JNK1/2
JNK1/2
P-TAK1
TAK1
GAPDH
43kDa
43kDa
42/44kDa
42/44kDa
46/54kDa
46/54kDa
70kDa
70kDa
37kDa
Protein/GAPDH (fold change)
P-P38
P-ERK
P-JNK
P-TAK1
AdshRNA PBS
AdshTRIM38 PBS
AdshRNA Ang-II
AdshTRIM38 Ang-II
D
PBS
Ang II
AdGFP
AdTRIM38
AdGFP
AdTRIM38
P-P38
P38
P-ERK1/2
ERK1/2
P-JNK1/2
JNK1/2
P-TAK1
TAK1
GAPDH
43kDa
43kDa
42/44kDa
42/44kDa
46/54kDa
46/54kDa
70kDa
70kDa
37kDa
Protein/GAPDH (fold change)
P-P38
P-ERK
P-JNK
P-TAK1
AdGFP PBS
AdTRIM38 PBS
AdGFP Ang-II
AdTRIM38 Ang-II

Figure 5. TRIM38 inactivates MAPK signaling during myocardial infarction

(A and B) Representative Western blotting (Up) and quantitative results (Down) of total (T-) and phospho- (P-) TAK1-p38/ERK1/2/JNK1/2 levels in mice myocardium subjected to sham or MI operation. n = 4–6/each group; *p < 0.05, **p < 0.01.
(C and D) Representative Western blotting (Up) and quantitative results (Down) results of total- (T-) and phospho- (P-) TAK1-p38/ERK1/2/JNK1/2 levels in NRCFs transfected with AdshTRIM38 or AdTRIM38 stimulated with angiotensin II. Three independent experiments. *p < 0.05, **p < 0.01. GAPDH was used as a loading control. The result was means ± S.D., and statistical analyses were performed using one-way ANOVA.

immunoprecipitated with an anti-TAK1 antibody, and the immunoprecipitates were immunoblotted with an anti-ubiquitin antibody. The ubiquitination level of TAK1 increased after angiotensin II stimulation (Figure 7A). Interestingly, TRIM38 overexpression had little effect on the K48-linked ubiquitination of TAK1, but it substantially suppressed the total ubiquitination and K63-linked ubiquitination of TAK1 (Figure 7A). The results showed that TRIM38 inhibited K63-linked ubiquitination of endogenous TAK1, but not K48-linked ubiquitin chains in CFs. E3 ubiquitin ligase activity cannot explain this function of TRIM38. Therefore, we speculated that TRIM38 interacts with other substrates to indirectly regulate TAK1 ubiquitination. Several studies have shown that TAB2/3 bind to K63-linked polyubiquitination, which is critical for TAK1 activation (Shibuya et al., 1996; Xu and Lei, 2020). Thus, we hypothesized that TRIM38 targeted the TAK1-TAB2/3 complex to regulate cardiac fibrosis. Immunofluorescence staining revealed that TRIM38 and TAB2/3 were completely colocalized in the cytoplasm of HEK293T cells (Figure 7B). Furthermore, immunoprecipitation analysis showed that exogenous FLAG-tagged TRIM38 interacted with HA-tagged TAB2/3 and Myc-tagged TAK1 (Figure 7C). Consistently, after exposure to angiotensin II, endogenous TAB2/3 co-precipitated with endogenous TRIM38 in CF cell extracts (Figure 7D). Furthermore, we examined the effect of TRIM38 on the individual levels of TAK1-TAB2/3 complex components. TRIM38 knockdown increased TAB2/3 protein levels in both unstimulated and angiotensin II-stimulated conditions compared to those in the AdshRNA-infected group (Figure 7E). These results confirmed the function of TRIM38 in TAB2/3 degradation in CFs under physiological conditions. Furthermore, we found that the protein levels of HA-TAB2/3, but not Myc-TAK1, were correlated with the level of FLAG-TRIM38 in a dose-dependent manner (Figures 7F and S5). Overexpression of FLAG-TRIM38 decreased HA-TAB2/3 protein levels in a dose-dependent manner (Figure 7F). The ubiquitin-proteasome and lysosome pathways are major routes for regulating protein stability (Hu et al., 2014). To determine the degradation pathway of TAB2/3, we used MG132 and chloroquine to inhibit the proteasomal and lysosomal degradation pathways, respectively, in HEK293T cells. Our results showed that TRIM38-mediated degradation of TAB2/3 was completely inhibited by chloroquine but not by the proteasome inhibitor MG132 (Figure 7G). This indicated that TAB2/3 degradation is lysosome-dependent rather than proteasome-dependent. As TRIM38 dephosphorylates and inactivates TAK1 kinase, we examined whether TRIM38 overexpression could affect Myc-TAK1 and HA-TAB2/3 co-overexpression-induced TAK1 phosphorylation. As expected, the results suggested that HEK293T cells co-expressing HA-TAB2/3 and Myc-TAK1 promoted the phosphorylation of TAK1 (lane 2). Co-expression with FLAG-TRIM38 (lane 3) greatly decreased the phosphorylation of endogenous TAK1 (Figure 7H). Given the interaction between TRIM38 and the TAK1-TAB2/3 complex and the effect of TRIM38 on the stability of the TAB2/3 protein, we speculated that TRIM38 inhibits the ubiquitination of TAK1 by affecting the TAB2/3 protein level. To test this hypothesis, HEK293T cells were co-transfected with the indicated plasmids. Co-immunoprecipitation analyses showed that Myc-TAK1 was K63-ubiquitinated by HA-TAB2/3, and K63-linked ubiquitination of Myc-TAK1 significantly decreased in the presence of FLAG-TRIM38 (Figures 7I and 7J). The results showed that the interaction between TRIM38 and TAB2/3 inhibited K63-linked ubiquitination of TAK1. Together, these findings indicate that TRIM38 suppresses K63-linked polyubiquitin and TAK1 activity by mediating TAB2/3 degradation.

DISCUSSION

TRIM38 is an important member of the TRIM protein family, a group of E3 ubiquitin ligases that regulate intracellular protein homeostasis by mediating the ubiquitination of substrate proteins. TRIM38 is widely expressed in immune and tumor cells and is involved in pathological processes such as bone proliferation, tumorigenesis, and autoimmune diseases. However, the effect of TRIM38 on cardiac fibrosis and heart failure has not yet been determined. In this study, we examined the potential function of TRIM38 in MI-induced cardiac fibrosis through genetic manipulation of TRIM38 expression *in vivo* and *in vitro*. In patients with AMI, mouse heart after MI, and angiotensin II-treated CFs, TRIM38 expression was significantly decreased. Functional experiments confirmed that TRIM38 overexpression protected mouse hearts from pathological fibrosis and dysfunction caused by MI. Conversely, decreased TRIM38 expression was related to an excessive cardiac fibrosis response and exacerbated cardiac dysfunction. Finally, we verified that TRIM38 exerts

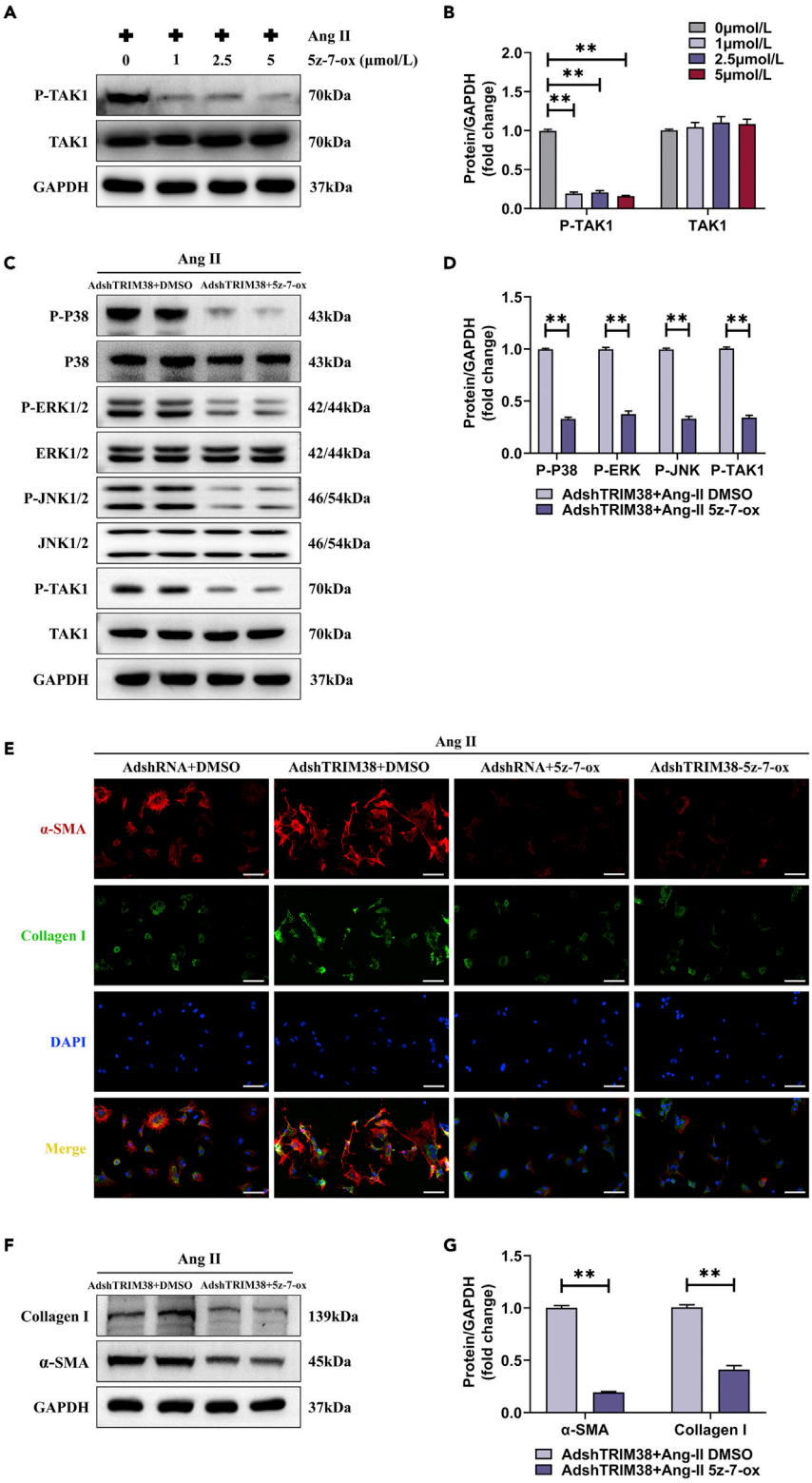
A
Ang II
0 1 2.5 5
5z-7-ox (μmol/L)
P-TAK1
TAK1
GAPDH
70kDa
70kDa
37kDa
B
0μmol/L
1μmol/L
2.5μmol/L
5μmol/L
Protein/GAPDH (fold change)
P-TAK1
TAK1
C
Ang II
AdshTRIM38+DMSO
AdshTRIM38+5z-7-ox
P-P38
P38
P-ERK1/2
ERK1/2
P-JNK1/2
JNK1/2
P-TAK1
TAK1
GAPDH
43kDa
43kDa
42/44kDa
42/44kDa
46/54kDa
46/54kDa
70kDa
70kDa
37kDa
D
Protein/GAPDH (fold change)
P-P38
P-ERK
P-JNK
P-TAK1
AdshTRIM38+Ang-II DMSO
AdshTRIM38+Ang-II 5z-7-ox
E
Ang II
AdshRNA+DMSO
AdshTRIM38+DMSO
AdshRNA+5z-7-ox
AdshTRIM38-5z-7-ox
α-SMA
Collagen I
DAPI
Merge
F
Ang II
AdshTRIM38+DMSO
AdshTRIM38+5z-7-ox
Collagen I
α-SMA
GAPDH
139kDa
45kDa
37kDa
G
Protein/GAPDH (fold change)
α-SMA
Collagen I
AdshTRIM38+Ang-II DMSO
AdshTRIM38+Ang-II 5z-7-ox

Figure 6. Blockage of TAK1/MAPK signaling pathways rescues the transformation of cardiac fibroblasts to myofibroblasts induced by angiotensin II

(A and B) Representative Western blotting (Left) and quantitative results (Right) of total- (T-) and phospho- (P-) TAK1 levels in NRCFs. NRCFs treated with angiotensin II in the presence or absence of 5z-7-ox (1, 2.5, and 5 μmol/L). Three independent experiments. **p < 0.01.

(C and D) Representative Western blotting (Left) and quantitative results (Right) of total (T-) and phospho- (P-) TAK1-p38/ERK1/2/JNK1/2 levels in AdshTRIM38-NRCFs treated with 5z-7-ox or DMSO, and followed by angiotensin II treatment. Three independent experiments. **p < 0.01.

(E) Representative immunofluorescence staining image of collagen I and α-SMA in NRCFs transfected with AdshRNA or AdshTRIM38 treated with 5z-7-ox or DMSO, and followed by angiotensin II treatment. Scale bar = 200 μm.

(F and G) Representative Western blotting (Left) and quantitative results (Right) of collagen I and α-SMA protein expression in the AdshTRIM38 NRCFs treated with 5z-7-ox or DMSO, and followed by angiotensin II treatment. Three independent experiments. **p < 0.01. Abbreviations: 5z-7-ox, 5z-7-oxozeaneol; DMSO, dimethyl sulfoxide. The result was means ± S.D., and statistical analyses were performed using one-way ANOVA.

its anti-fibrotic effect by inhibiting the TAK1/MAPK pathway, via targeting TAB2/3 degradation. In conclusion, we have provided the first *in vivo* evidence that TRIM38 is a negative regulator of cardiac remodeling.

In this study, we first observed a decrease in TRIM38 expression in post-MI fibrotic hearts. Downregulation of TRIM38 expression was negatively correlated with cardiac fibroblast activation in CFs treated with angiotensin II, indicating that TRIM38 deficiency is related to the progression of pathological cardiac fibrosis. In subsequent experiments, we adopted gain-of-function and loss-of-function methods. Our *in vivo* results showed that TRIM38 deficiency exacerbated MI-induced fibrosis and pathological remodeling, whereas TRIM38 overexpression had the opposite effect *in vivo*. Additionally, *in vitro* experiments revealed that TRIM38 knockdown significantly exacerbated angiotensin II-induced CF activation, whereas the upregulation of TRIM38 expression inhibited this fibrotic response. These data strongly suggest a cardioprotective effect of TRIM38 in pathological cardiac fibrosis, alleviating heart failure progression following MI.

The mechanism of action of TRIM38 has been explored in diverse fields. Hu et al. (2014) found that TRIM38 negatively regulates TNF- and IL-1β-induced activation of MAPK involved in inflammatory responses. In addition, there is extensive evidence to suggest that the MAPK signaling pathway plays a critical role in CF proliferation (Tao et al., 2016; Zhang and Liu, 2002). Thus, MAPK activation may be a key TRIM38 downstream signaling pathway. The three most widely characterized MAPK subfamilies are p38, ERK1/2, and JNK1/2. To elucidate the possible mechanism by which TRIM38 attenuates cardiac fibrosis, we examined the protein levels of phosphorylated p38, ERK1/2, and JNK1/2 following fibrosis stimulation. Western blot analysis showed that the levels of phosphorylated p38, ERK1/2, and JNK1/2 were further enhanced by TRIM38 knockdown in response to MI or angiotensin II treatment. Overexpression of TRIM38 effectively blocked p38, ERK1/2, and JNK1/2 activation. Among these kinases, JNK and p38 MAPK are collectively referred to as stress-activated protein kinases (Rose et al., 2010). P38 MAPK kinase is a major regulator of the cardiac fibrotic response (Molkentin et al., 2017). It has been shown that p38 MAPK kinase is involved in CF differentiation and can promote myofibroblast transformation during ischaemic injury or neurohumoral stimulation (Davis and Molkentin, 2014; Sinfield et al., 2013). The roles of ERK and JNK signaling in cardiac remodeling and heart failure are currently unclear. Although *in vitro* studies have reported that the inhibition of ERK1/2 and JNK1/2 kinases significantly attenuates collagen synthesis and alleviates fibrosis, *in vivo* evidence of ERK1/2 and JNK1/2 in the context of cardiac fibrosis is lacking (Du et al., 2020; Schafer et al., 2017). Our *in vivo* results suggest that the cardioprotective effect of TRIM38 may be related to its inhibition of the p38, ERK1/2, and JNK1/2 pathways.

TAK1 is a vital upstream activator of the MAPK signaling pathway and participates in the development of cardiac fibrosis (Bansal et al., 2017). We performed Western blotting to analyze whether TRIM38 regulates TAK1 signaling. Our results revealed that TRIM38 deficiency enhanced TAK1 activity, whereas its overexpression exerted the opposite effects. 5Z-7-oxozeaenol is a potent irreversible and selective inhibitor of TAK1 and has been widely used to confirm the specific role of TAK1 (Ninomiya-Tsuji et al., 2003). In our study, 5Z-7-oxozeaenol almost completely inhibited the activation of TAK1 and its downstream proteins p38, ERK1/2, and JNK1/2, and eliminated the pro-fibrotic effect of TRIM38 knockdown in response to angiotensin II treatment. Therefore, we conclude that the anti-fibrotic effects of TRIM38 may occur through the inhibition of the TAK1/MAPK axis.

TAB2 and TAB3 function as substrate adaptors and directly bind to TRAF6 and TAK1, leading to autophosphorylation and activation of TAK1, and further activation of NF-κB and MAPK (Huang et al., 2021). TAB2/3

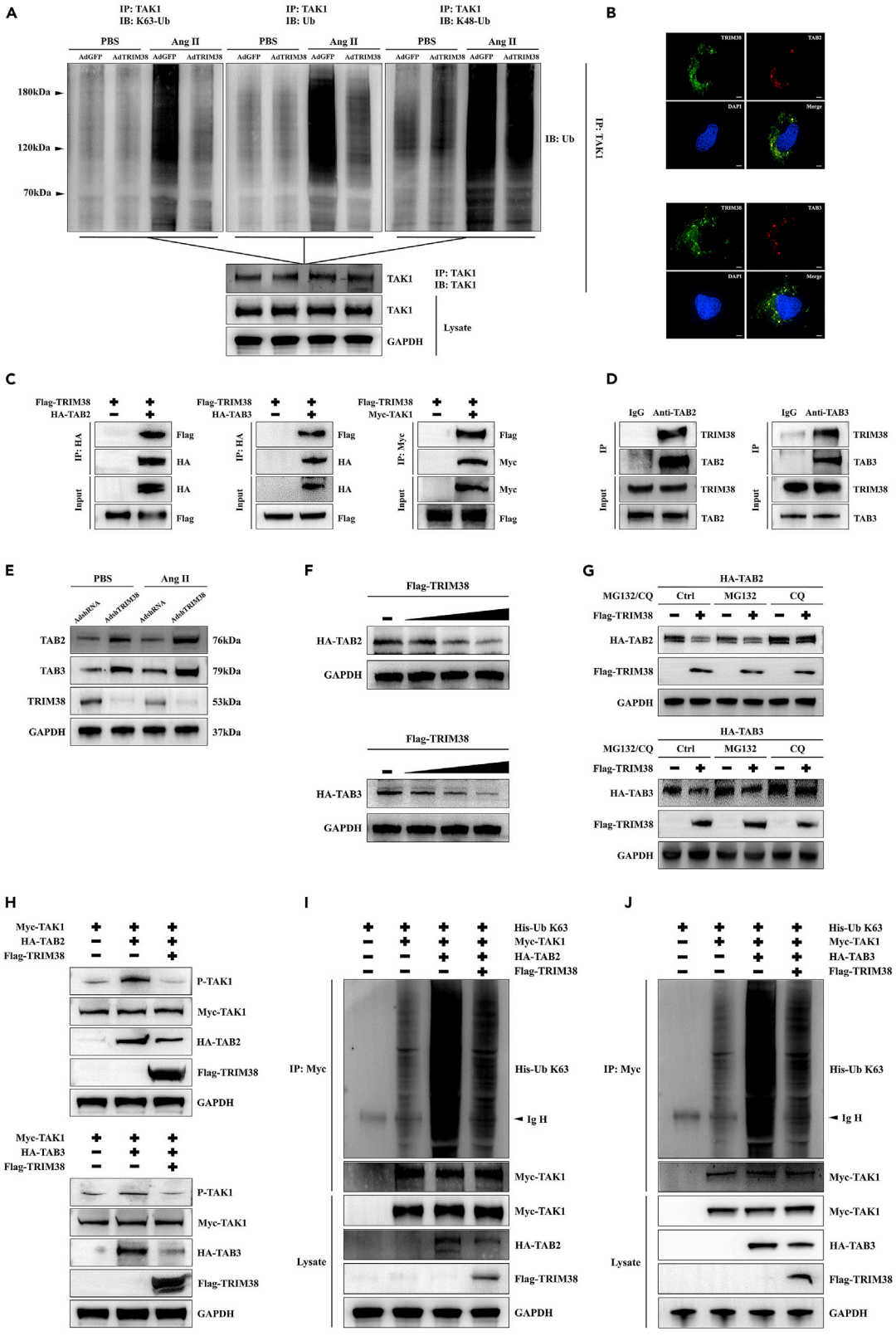
A
IP: TAK1
IB: K63-Ub
IP: TAK1
IB: Ub
IP: TAK1
IB: K48-Ub
PBS
Ang II
AdGFP
AdTRIM38
180kDa
120kDa
70kDa
IB: Ub
TAK1
IP: TAK1
IB: TAK1
TAK1
GAPDH
Lysate
B
IP: TAK1
TRIM38
TAB2
TAB3
DAPI
Merge
C
Flag-TRIM38
HA-TAB2
HA-TAB3
Myc-TAK1
IP: HA
IP: Myc
Input
Flag
HA
Myc
D
IgG
Anti-TAB2
Anti-TAB3
IP
Input
TRIM38
TAB2
TAB3
E
PBS
Ang II
AdshRNA
AdshTRIM38
TAB2
TAB3
TRIM38
GAPDH
76kDa
79kDa
53kDa
37kDa
F
Flag-TRIM38
HA-TAB2
HA-TAB3
GAPDH
G
HA-TAB2
HA-TAB3
MG132/CQ
Ctrl
MG132
CQ
Flag-TRIM38
GAPDH
H
Myc-TAK1
HA-TAB2
HA-TAB3
Flag-TRIM38
P-TAK1
GAPDH
I
J
His-Ub K63
Myc-TAK1
HA-TAB2
HA-TAB3
Flag-TRIM38
IP: Myc
Ig H
Lysate
GAPDH

Figure 7. TRIM38 suppresses TAK1 activity by mediating the degradation of TAB2/3

(A) NRCFs transfected with AdGFP or AdTRIM38 were cultured in the presence or absence of angiotensin II. Protein lysates were immunoprecipitated with TAK1-specific antibody and the equal amounts of immunoprecipitates were subjected to SDS–PAGE. Western blotting analysis was performed using anti-ubiquitin, anti-K63- or anti-K48-ubiquitin antibodies.

(B) The co-localization of TRIM38 and TAB2/3 in HEK293T cells. The staining of TRIM38 is green, TAB2/3 is red and DAPI is blue in representative confocal images.

(C) The TRIM38 and TAK1-TAB2/3 interaction was detected by immunoprecipitation (IP) assays. Flag-tagged TRIM38 and HA-tagged TAB2, Flag-tagged TRIM38 and HA-tagged TAB3 or Flag-tagged TRIM38 and Myc-tagged TAK1 plasmids were co-transfected into HEK293T. 48 h later, harvested cell lysates were subjected to IP with Anti-HA antibody or Anti-Myc antibody.

(D) Endogenous TRIM38 was precipitated using anti-TAB2 and anti-TAB3 antibodies in NRCFs.

(E) Western blot analysis of the expression of TAB2, TAB3, and TRIM38 in NRCFs transfected with AdshRNA or AdshTRIM38 and then stimulated with angiotensin II.

(F) Protein level of HA-tagged TAB2 and HA-tagged TAB3 in HEK293T cells transfected with increasing doses of Flag-tagged TRIM38 (1 ug, 2 ug, and 4 ug), HA-tagged TAB2, or HA-tagged TAB3 plasmids. GAPDH served as a loading control.

(G) Protein level of HA-tagged TAB2 and HA-tagged TAB3 in HEK293T cells co-transfected with Flag-tagged TRIM38, HA-tagged TAB2 or HA-tagged TAB3 plasmids and treated with MG132, CQ, or DMSO. GAPDH served as a loading control. Representative of three independent experiments.

(H) Combinations of Myc-TAK1, HA-TAB2, HA-TAB3, and Flag-TRIM38 were expressed in HEK293T cells and analyzed by immunoblotting. *Lanes one to three* show extracts from HEK293T cells co-expressing 1) Myc-TAK1, 2) Myc-TAK1 with HA-TAB2/3, or 3) Myc-TAK1 with HA-TAB2/3 and Flag-TRIM38.

(I and J) IP analyses of the K63 polyubiquitination of TAK1 from HEK293T cells expressing HA-tagged TAB2/3 and His-tagged K63-ubiquitin in the presence or absence of Flag-TRIM38. Abbreviations: Ctrl, control; DMSO, dimethyl sulfoxide.

can recognize the K63-linked ubiquitin chain of RIP1 in the TNFα signal or TRAF6 in the IL-1β signal and recruit TAK1 to the signalosome. Previous research by Hu et al. (2014) confirmed that TRIM38 promotes the degradation of TAB2 and TAB3, necessary for ubiquitin ligase activity, to prevent the persistent activation of TAK1. In light of the important role of ubiquitination in TAK1-TAB2/3-mediated signaling, upstream of MAPK signaling, we hypothesized that TRIM38 exerts its effect at the level of the TAK1-TAB2/3 complex. In the present study, we found that TRIM38 negatively regulated TAK1 activation by inhibiting its K63-linked polyubiquitin state. This effect does not seem to be explained by the E3 ligase activity of TRIM38, suggesting that it may indirectly regulate the activation of TAK1 by interacting with other molecules. Therefore, we examined whether TRIM38 interacts with TAK1 and TAB2/3. Immunofluorescence staining and co-IP experiments suggested that TRIM38 interacted with TAK1-TAB2/3 and catalyzed the degradation of TAB2/3. More importantly, we found that endogenous TRIM38 co-immunoprecipitated with the anti-TAB2/3 antibody in CFs. Furthermore, TAB2/3-potentiated phosphorylation of TAK1 was attenuated after TRIM38 overexpression, indicating that TRIM38 inhibited TAB2/3-mediated phosphorylation of TAK1. Notably, we discovered for the first time that the E3 ligase TRIM38 binds to TAB2/3 and impedes TAK1 activation in CFs. This finding extends the function of TRIM38 as an inhibitor of TAK1 activation in response to cardiac fibrosis, which may be a promising therapeutic strategy.

A previous study confirmed that TRIM38 inhibits TNF-α- and IL-1β-triggered NF-κB activation by mediating lysosome-dependent degradation of TAB2/3, leading to a decrease in TAK1 activity. This was consistent with our finding that TRIM38-mediated degradation of TAB2/3 was completely impeded by an inhibitor of the lysosome (chloroquine), but not by a proteasome inhibitor (MG132). Furthermore, increased concentrations of TRIM38 also suppressed TAB2/3 expression. We performed ubiquitination assays and observed that TAB-potentiated K63-linked polyubiquitination of TAK1 was largely eliminated in the presence of TRIM38. Further experiments showed that TRIM38-mediated degradation of TAB2/3 could not be blocked by MG132. This indicates that TAB2/3 degradation is independent of the 26S proteasome pathway. The specific underlying mechanism leading to this result is unclear. Here, TRIM38 may function as an adaptor by affecting protein-protein interactions in lysosome-associated TAB2/3 degradation. The E3 ubiquitin ligase TRIM38 mediates the protein stability of TAB2/3 through the lysosomal pathway, which warrants further study.

Over the last few years, a precise link has been established between the regulation of cardiac fibrosis and epigenetic modifying enzymes, such as the sirtuin SIRT3, which exerts an antioxidant response by maintaining mitochondrial homeostasis, increasing ATP levels in body cells as well as stimulatory and anti-fibrotic functions (Liu et al., 2019a). Overexpression of the methyltransferase METTL3 aggravates collagen deposition *in vivo*, and silencing of METTL3 reduces the level of m^6A modification of fibrosis-related genes and significantly attenuates cardiac fibrosis in MI mice (Li et al., 2021). Furthermore, a recent study revealed a novel signaling cascade, METTL3/MALAT1/PTBP1/USP8/TAK1, which aggravates liver fibrosis by activating M1 macrophage polarization (Shu et al., 2021). This involves interactions between epigenetic factors

and post-transcriptional and post-translational modifications including methylation, ubiquitination, and signal transduction, which affect the pathological mechanism of cardiac fibrosis. Here, we linked the E3 ubiquitin ligase TRIM38 to cardiac fibrosis. This lays the foundation for future detailed studies on the synergistic effects of different protein modifications in cardiac fibrosis after MI. Although the exact mechanism is unclear, there is a potential explanation for the decrease in TRIM38 expression observed during cardiac fibrosis. Based on the fact that TRIM38 is capable of self-ubiquitination, it is hypothesized that fibrotic stimulation may decrease TRIM38 stability (Liu et al., 2011). TRIM38 expression may be reduced by self-association-based self-ubiquitination and subsequent proteasomal degradation. However, additional research is required to test our hypotheses.

In conclusion, we discovered that TRIM38 is a novel suppressor of TAK1 activation in the setting of MI. Cardiac TRIM38 mediates the degradation of TAB2/3 and inhibition of the downstream TAK1/MAPK signaling pathway, leading to remission of cardiac fibrosis. This signaling cascade offers a series of potentially novel therapeutic targets for the treatment of cardiac fibrosis and dysfunction.

Limitations of the study

This study has the following limitations. Firstly, although our data show that TRIM38 is downregulated in the blood of patients with MI, its function in human cardiac injury remains unknown. Furthermore, neonatal CFs behave substantially differently from adult CFs. Therefore, our findings need to be verified in adult CFs. Third, adeno-associated virus-mediated changes in cardiomyocyte TRIM38 expression may affect the cardiac phenotype in mice. Thus, the potential involvement of other factors (proteins/RNAs) in the regulation of myocardial fibrosis by TRIM38 cannot be ruled out.

STAR★METHODS

Detailed methods are provided in the online version of this paper and include the following:

- KEY RESOURCES TABLE
- RESOURCE AVAILABILITY
  - Lead contact
  - Materials availability
  - Data and code availability
- EXPERIMENTAL MODEL AND SUBJECT DETAILS
  - Patient samples
  - Animal experiments
  - MI models
  - Isolation and culture of primary CFs
- METHOD DETAILS
  - Adenovirus infection
  - Western blot analysis
  - Immunofluorescence staining
  - Total RNA isolation and quantitative real-time PCR
  - Wound healing assay
  - AAV9-mediated gene delivery in the heart
  - Histopathology assay
  - Echocardiography analysis
  - Plasmid transfection
  - IP assays
  - Ubiquitination assay
- QUANTIFICATION AND STATISTICAL ANALYSIS

SUPPLEMENTAL INFORMATION

Supplemental information can be found online at https://doi.org/10.1016/j.isci.2022.104780.

ACKNOWLEDGMENTS

The authors are grateful to the staff of the Institute of Cardiovascular Disease at Southeast University. Funding for the study was provided by the National Nature Science Foundation of China [No. 81770231 and No.

81270203]; the Natural Science Foundation of Jiangsu [No. BK20161436]; Jiangsu Province Key Medical Research Project [No. K2019006]; Jiangsu Provincial Key Medical Discipline [No. ZDXKA2016023]; and Jiangsu Provincial Key Research and Development Program [No. BE2016785].

AUTHOR CONTRIBUTIONS

Zhengri Lu designed the research, performed experiments, and data analysis, and wrote the article. Chunshu Hao and Hao Qian performed experiments and data analysis. Yuanyuan Zhao and Xiangwei Bo analyzed the data. Genshan Ma and Yuyu Yao designed the overall research. Lijuan Chen designed the overall research, analyzed data, and contributed to article drafting.

DECLARATION OF INTERESTS

The authors declare no competing interests.

Received: December 26, 2021
Revised: June 27, 2022
Accepted: July 13, 2022
Published: August 19, 2022

REFERENCES

Ajibade, A.A., Wang, H.Y., and Wang, R.F. (2013). Cell type-specific function of TAK1 in innate immune signaling. Trends Immunol. *34*, 307–316. https://doi.org/10.1016/j.it.2013.03.007.

Akira, S. (2003). Toll-like receptor signaling. J. Biol. Chem. *278*, 38105–38108. https://doi.org/10.1074/jbc.R300028200.

Bansal, T., Chatterjee, E., Singh, J., Ray, A., Kundu, B., Thankamani, V., Sengupta, S., and Sarkar, S. (2017). Arjunolic acid, a peroxisome proliferator-activated receptor alpha agonist, regresses cardiac fibrosis by inhibiting non-canonical TGF-beta signaling. J. Biol. Chem. *292*, 16440–16462. https://doi.org/10.1074/jbc.M117.788299.

Borlepawar, A., Rangrez, A.Y., Bernt, A., Christen, L., Sossalla, S., Frank, D., and Frey, N. (2017). TRIM24 protein promotes and TRIM32 protein inhibits cardiomyocyte hypertrophy via regulation of dysbindin protein levels. J. Biol. Chem. *292*, 10180–10196. https://doi.org/10.1074/jbc.M116.752543.

Chen, L., Huang, J., Ji, Y., Zhang, X., Wang, P., Deng, K., Jiang, X., Ma, G., and Li, H. (2016). Tripartite motif 32 prevents pathological cardiac hypertrophy. Clin. Sci. *130*, 813–828. https://doi.org/10.1042/CS20150619.

Chen, L., Huang, J., Ji, Y.X., Mei, F., Wang, P.X., Deng, K.Q., Jiang, X., Ma, G., and Li, H. (2017). Tripartite motif 8 contributes to pathological cardiac hypertrophy through enhancing transforming growth factor beta-activated kinase 1-dependent signaling pathways. Hypertension *69*, 249–258. https://doi.org/10.1161/HYPERTENSIONAHA.116.07741.

Criollo, A., Niso-Santano, M., Malik, S.A., Michaud, M., Morselli, E., Mariño, G., Lachkar, S., Arkhipenko, A.V., Harper, F., Pierron, G., et al. (2011). Inhibition of autophagy by TAB2 and TAB3. EMBO J. *30*, 4908–4920. https://doi.org/10.1038/emboj.2011.413.

Davis, J., and Molkentin, J.D. (2014). Myofibroblasts: trust your heart and let fate decide. J. Mol. Cell. Cardiol. *70*, 9–18. https://doi.org/10.1016/j.yjmcc.2013.10.019.

Du, Y., Xiao, H., Wan, J., Wang, X., Li, T., Zheng, S., Feng, J., Ye, Q., Li, J., Li, G., and Fan, Z. (2020). Atorvastatin attenuates TGFbeta1induced fibrogenesis by inhibiting Smad3 and MAPK signaling in human ventricular fibroblasts. Int. J. Mol. Med. *46*, 633–640. https://doi.org/10.3892/ijmm.2020.4607.

Frangogiannis, N.G. (2019). Cardiac fibrosis: cell biological mechanisms, molecular pathways and therapeutic opportunities. Mol. Aspects Med. *65*, 70–99. https://doi.org/10.1016/j.mam.2018.07.001.

Frangogiannis, N.G. (2021). Cardiac fibrosis. Cardiovasc. Res. *117*, 1450–1488. https://doi.org/10.1093/cvr/cvaa324.

Guo, J., Jia, F., Jiang, Y., Li, Q., Yang, Y., Xiao, M., and Xiao, H. (2018). Potential role of MG53 in the regulation of transforming-growth-factor-beta1-induced atrial fibrosis and vulnerability to atrial fibrillation. Exp. Cell Res. *362*, 436–443. https://doi.org/10.1016/j.yexcr.2017.12.007.

Hao, C., Lu, Z., Zhao, Y., Chen, Z., Shen, C., Ma, G., and Chen, L. (2020). Overexpression of GATA4 enhances the antiapoptotic effect of exosomes secreted from cardiac colony-forming unit fibroblasts via miRNA221-mediated targeting of the PTEN/PI3K/AKT signaling pathway. Stem Cell Res. Ther. *11*, 251. https://doi.org/10.1186/s13287-020-01759-8.

Hatakeyama, S. (2017). TRIM family proteins: roles in autophagy, immunity, and carcinogenesis. Trends Biochem. Sci. *42*, 297–311. https://doi.org/10.1016/j.tibs.2017.01.002.

Hu, M.M., Yang, Q., Zhang, J., Liu, S.M., Zhang, Y., Lin, H., Huang, Z.F., Wang, Y.Y., Zhang, X.D., Zhong, B., and Shu, H.B. (2014). TRIM38 inhibits TNFalpha- and IL-1beta-triggered NF-kappaB activation by mediating lysosome-dependent degradation of TAB2/3. Proc. Natl. Acad. Sci. USA *111*, 1509–1514. https://doi.org/10.1073/pnas.1318227111.

Hu, M.M., Xie, X.Q., Yang, Q., Liao, C.Y., Ye, W., Lin, H., and Shu, H.B. (2015). TRIM38 negatively regulates TLR3/4-mediated innate immune and inflammatory responses by two sequential and distinct mechanisms. J. Immunol. *195*, 4415–4425. https://doi.org/10.4049/jimmunol.1500859.

Huang, C., Liu, Q., Tang, Q., Jing, X., Wu, T., Zhang, J., Zhang, G., Zhou, J., Zhang, Z., Zhao, Y., et al. (2021). Hepatocyte-specific deletion of Nlrp6 in mice exacerbates the development of non-alcoholic steatohepatitis. Free Radic. Biol. Med. *169*, 110–121. https://doi.org/10.1016/j.freeradbiomed.2021.04.008.

Ishitani, T., Takaesu, G., Ninomiya-Tsuji, J., Shibuya, H., Gaynor, R.B., and Matsumoto, K. (2003). Role of the TAB2-related protein TAB3 in IL-1 and TNF signaling. EMBO J. *22*, 6277–6288. https://doi.org/10.1093/emboj/cdg605.

Kawai, T., and Akira, S. (2006). TLR signaling. Cell Death Differ. *13*, 816–825. https://doi.org/10.1038/sj.cdd.4401850.

Kim, S.Y., Shim, J.H., Chun, E., and Lee, K.Y. (2012). Reciprocal inhibition between the transforming growth factor-beta-activated kinase 1 (TAK1) and apoptosis signal-regulating kinase 1 (ASK1) mitogen-activated protein kinase kinase kinases and its suppression by TAK1-binding protein 2 (TAB2), an adapter protein for TAK1. J. Biol. Chem. *287*, 3381–3391. https://doi.org/10.1074/jbc.M111.317875.

Koitabashi, N., Danner, T., Zaiman, A.L., Pinto, Y.M., Rowell, J., Mankowski, J., Zhang, D., Nakamura, T., Takimoto, E., and Kass, D.A. (2011). Pivotal role of cardiomyocyte TGF-beta signaling in the murine pathological response to sustained pressure overload. J. Clin. Invest. *121*, 2301–2312. https://doi.org/10.1172/JCI44824.

Kong, P., Christia, P., and Frangogiannis, N.G. (2014). The pathogenesis of cardiac fibrosis. Cell. Mol. Life Sci. *71*, 549–574. https://doi.org/10.1007/s00018-013-1349-6.

Lee, Y.R., Chen, M., Lee, J.D., Zhang, J., Lin, S.Y., Fu, T.M., Chen, H., Ishikawa, T., Chiang, S.Y.,

Katon, J., et al. (2019). Reactivation of PTEN tumor suppressor for cancer treatment through inhibition of a MYC-WWP1 inhibitory pathway. Science *364*, eaau0159. https://doi.org/10.1126/science.aau0159.

Li, L., Zhao, Q., and Kong, W. (2018). Extracellular matrix remodeling and cardiac fibrosis. Matrix Biol. *68–69*, 490–506. https://doi.org/10.1016/j.matbio.2018.01.013.

Li, T., Zhuang, Y., Yang, W., Xie, Y., Shang, W., Su, S., Dong, X., Wu, J., Jiang, W., Zhou, Y., et al. (2021). Silencing of METTL3 attenuates cardiac fibrosis induced by myocardial infarction via inhibiting the activation of cardiac fibroblasts. FASEB J. *35*, e21162. https://doi.org/10.1096/fj.201903169R.

Liu, X., Lei, X., Zhou, Z., Sun, Z., Xue, Q., Wang, J., and Hung, T. (2011). Enterovirus 71 induces degradation of TRIM38, a potential E3 ubiquitin ligase. Virol. J. *8*, 61. https://doi.org/10.1186/1743-422X-8-61.

Liu, F., Song, R., Feng, Y., Guo, J., Chen, Y., Zhang, Y., Chen, T., Wang, Y., Huang, Y., Li, C.Y., et al. (2015a). Upregulation of MG53 induces diabetic cardiomyopathy through transcriptional activation of peroxisome proliferation-activated receptor alpha. Circulation *131*, 795–804. https://doi.org/10.1161/CIRCULATIONAHA.114.012285.

Liu, J., Zhu, H., Zheng, Y., Xu, Z., Li, L., Tan, T., Park, K.H., Hou, J., Zhang, C., Li, D., et al. (2015b). Cardioprotection of recombinant human MG53 protein in a porcine model of ischemia and reperfusion injury. J. Mol. Cell. Cardiol. *80*, 10–19. https://doi.org/10.1016/j.yjmcc.2014.12.010.

Liu, J., Yan, W., Zhao, X., Jia, Q., Wang, J., Zhang, H., Liu, C., He, K., and Sun, Z. (2019a). Sirt3 attenuates post-infarction cardiac injury via inhibiting mitochondrial fission and normalization of AMPK-Drp1 pathways. Cell. Signal. *53*, 1–13. https://doi.org/10.1016/j.cellsig.2018.09.009.

Liu, W., Wang, G., Zhang, C., Ding, W., Cheng, W., Luo, Y., Wei, C., and Liu, J. (2019b). MG53, A novel regulator of KChIP2 and Ito, f, plays a critical role in electrophysiological remodeling in cardiac hypertrophy. Circulation *139*, 2142–2156. https://doi.org/10.1161/CIRCULATIONAHA.118.029413.

Matsuda, A., Suzuki, Y., Honda, G., Muramatsu, S., Matsuzaki, O., Nagano, Y., Doi, T., Shimotohno, K., Harada, T., Nishida, E., et al. (2003). Large-scale identification and characterization of human genes that activate NF-kappaB and MAPK signaling pathways. Oncogene *22*, 3307–3318. https://doi.org/10.1038/sj.onc.1206406.

McNab, F.W., Rajsbaum, R., Stoye, J.P., and O'Garra, A. (2011). Tripartite-motif proteins and innate immune regulation. Curr. Opin. Immunol. *23*, 46–56. https://doi.org/10.1016/j.coi.2010.10.021.

Molkentin, J.D., Bugg, D., Ghearing, N., Dorn, L.E., Kim, P., Sargent, M.A., Gunaje, J., Otsu, K., and Davis, J. (2017). Fibroblast-specific genetic manipulation of p38 mitogen-activated protein kinase in vivo reveals its central regulatory role in fibrosis. Circulation *136*, 549–561. https://doi.org/10.1161/CIRCULATIONAHA.116.026238.

Ninomiya-Tsuji, J., Kajino, T., Ono, K., Ohtomo, T., Matsumoto, M., Shiina, M., Mihara, M., Tsuchiya, M., and Matsumoto, K. (2003). A resorcylic acid lactone, 5Z-7-oxozeaenol, prevents inflammation by inhibiting the catalytic activity of TAK1 MAPK kinase kinase. J. Biol. Chem. *278*, 18485–18490. https://doi.org/10.1074/jbc.M207453200.

Rose, B.A., Force, T., and Wang, Y. (2010). Mitogen-activated protein kinase signaling in the heart: angels versus demons in a heart-breaking tale. Physiol. Rev. *90*, 1507–1546. https://doi.org/10.1152/physrev.00054.2009.

Rupérez, M., Rodrigues-Díez, R., Blanco-Colio, L.M., Sánchez-López, E., Rodríguez-Vita, J., Esteban, V., Carvajal, G., Plaza, J.J., Egido, J., and Ruiz-Ortega, M. (2007). HMG-CoA reductase inhibitors decrease angiotensin II-induced vascular fibrosis: role of RhoA/ROCK and MAPK pathways. Hypertension *50*, 377–383. https://doi.org/10.1161/HYPERTENSIONAHA.107.091264.

Schafer, S., Viswanathan, S., Widjaja, A.A., Lim, W.W., Moreno-Moral, A., DeLaughter, D.M., Ng, B., Patone, G., Chow, K., Khin, E., et al. (2017). IL-11 is a crucial determinant of cardiovascular fibrosis. Nature *552*, 110–115. https://doi.org/10.1038/nature24676.

Schnee, J.M., and Hsueh, W.A. (2000). Angiotensin II, adhesion, and cardiac fibrosis. Cardiovasc. Res. *46*, 264–268. https://doi.org/10.1016/s0008-6363(00)00044-4.

Shi, M., Deng, W., Bi, E., Mao, K., Ji, Y., Lin, G., Wu, X., Tao, Z., Li, Z., Cai, X., et al. (2008). TRIM30 alpha negatively regulates TLR-mediated NF-kappa B activation by targeting TAB2 and TAB3 for degradation. Nat. Immunol. *9*, 369–377. https://doi.org/10.1038/ni1577.

Shibuya, H., Yamaguchi, K., Shirakabe, K., Tonegawa, A., Gotoh, Y., Ueno, N., Irie, K., Nishida, E., and Matsumoto, K. (1996). TAB1: an activator of the TAK1 MAPKKK in TGF-beta signal transduction. Science *272*, 1179–1182. https://doi.org/10.1126/science.272.5265.1179.

Shu, B., Zhou, Y.X., Li, H., Zhang, R.Z., He, C., and Yang, X. (2021). The METTL3/MALAT1/PTBP1/USP8/TAK1 axis promotes pyroptosis and M1 polarization of macrophages and contributes to liver fibrosis. Cell Death Discov. *7*, 368. https://doi.org/10.1038/s41420-021-00756-x.

Sinfield, J.K., Das, A., O'Regan, D.J., Ball, S.G., Porter, K.E., and Turner, N.A. (2013). p38 MAPK alpha mediates cytokine-induced IL-6 and MMP-3 expression in human cardiac fibroblasts. Biochem. Biophys. Res. Commun. *430*, 419–424. https://doi.org/10.1016/j.bbrc.2012.11.071.

Tao, H., Chen, Z.W., Yang, J.J., and Shi, K.H. (2016). MicroRNA-29a suppresses cardiac fibroblasts proliferation via targeting VEGF-A/MAPK signal pathway. Int. J. Biol. Macromol. *88*, 414–423. https://doi.org/10.1016/j.ijbiomac.2016.04.010.

Thygesen, K., Alpert, J.S., Jaffe, A.S., Chaitman, B.R., Bax, J.J., Morrow, D.A., and White, H.D.; Executive Group on behalf of the Joint European Society of Cardiology ESC/American College of Cardiology ACC/American Heart Association AHA/World Heart Federation WHF Task Force for the Universal Definition of Myocardial Infarction (2018). Fourth universal definition of myocardial infarction (2018). J. Am. Coll. Cardiol. *72*, 2231–2264. https://doi.org/10.1016/j.jacc.2018.08.1038.

Tian, X., Sun, C., Wang, X., Ma, K., Chang, Y., Guo, Z., and Si, J. (2020). ANO1 regulates cardiac fibrosis via ATI-mediated MAPK pathway. Cell Calcium *92*, 102306. https://doi.org/10.1016/j.ceca.2020.102306.

Travers, J.G., Kamal, F.A., Robbins, J., Yutzey, K.E., and Blaxall, B.C. (2016). Cardiac fibrosis: the fibroblast awakens. Circ. Res. *118*, 1021–1040. https://doi.org/10.1161/CIRCRESAHA.115.306565.

van Berlo, J.H., Maillet, M., and Molkentin, J.D. (2013). Signaling effectors underlying pathologic growth and remodeling of the heart. J. Clin. Invest. *123*, 37–45. https://doi.org/10.1172/JCI62839.

Xu, Y.R., and Lei, C.Q. (2020). TAK1-TABs complex: a central signalosome in inflammatory responses. Front. Immunol. *11*, 608976. https://doi.org/10.3389/fimmu.2020.608976.

Zhang, D., Gaussin, V., Taffet, G.E., Belaguli, N.S., Yamada, M., Schwartz, R.J., Michael, L.H., Overbeek, P.A., and Schneider, M.D. (2000). TAK1 is activated in the myocardium after pressure overload and is sufficient to provoke heart failure in transgenic mice. Nat. Med. *6*, 556–563. https://doi.org/10.1038/75037.

Zhang, W., and Liu, H.T. (2002). MAPK signal pathways in the regulation of cell proliferation in mammalian cells. Cell Res. *12*, 9–18. https://doi.org/10.1038/sj.cr.7290105.

STAR★METHODS

KEY RESOURCES TABLE

REAGENT or RESOURCE	SOURCE	IDENTIFIER
Antibodies		
Mouse monoclonal anti-TRIM38	Thermo Fisher Scientific	Cat#MA5-26235; RRID: AB_2723734
Rabbit polyclonal anti-TRIM38	Affinity Biosciences	Cat#AF0307; RRID: AB_2833471
Rabbit monoclonal anti-Collagen I	Abcam	Cat#ab270993
Mouse monoclonal anti-α-SMA	Abcam	Cat#ab7817; RRID: AB_262054
Rabbit monoclonal anti-Phospho-p44/42 MAPK (Erk1/2) (Thr202/Tyr204) (D13.14.4E)	Cell Signaling Technology	Cat#4370; RRID: AB_2315112
Rabbit monoclonal anti-p44/42 MAPK (Erk1/2) (137F5)	Cell Signaling Technology	Cat#4695; RRID: AB_390779
Rabbit monoclonal anti-Phospho-SAPK/JNK (Thr183/Tyr185) (81E11)	Cell Signaling Technology	Cat#4668; RRID: AB_823588
Rabbit polyclonal anti-SAPK/JNK	Cell Signaling Technology	Cat#9252; RRID: AB_2250373
Rabbit monoclonal anti-Phospho-p38 MAPK (Thr180/Tyr182) (D3F9)	Cell Signaling Technology	Cat#4511; RRID: AB_2139682
Rabbit polyclonal anti-p38 MAPK	Cell Signaling Technology	Cat#9212; RRID: AB_330713
Rabbit polyclonal anti-Phospho-TAK1 (Ser412)	Cell Signaling Technology	Cat#9339; RRID: AB_2140096
Rabbit polyclonal anti-Phospho-TAK1 (Thr184/Thr187)	Affinity Biosciences	Cat#AF4379; RRID: AB_2844444
Rabbit polyclonal anti-TAK1	Cell Signaling Technology	Cat#4505; RRID: AB_490858
Rabbit monoclonal anti-TAB2 (C88H10)	Cell Signaling Technology	Cat#3745; RRID: AB_2297368
Mouse monoclonal anti-TAB3 Antibody (D-9)	Santa Cruz	Cat#sc-166538; RRID: AB_2140515
Rabbit monoclonal anti-HA-Tag (C29F4)	Cell Signaling Technology	Cat#3724; RRID: AB_1549585
Mouse monoclonal anti-Myc-Tag (9B11)	Cell Signaling Technology	Cat#2276; RRID: AB_331783
Rabbit monoclonal anti-His-Tag (D3I1O)	Cell Signaling Technology	Cat#12698; RRID: AB_2744546
Rabbit monoclonal anti-DYKDDDDK Tag (D6W5B)	Cell Signaling Technology	Cat#14793; RRID: AB_2572291
Mouse monoclonal anti-GAPDH [6C5]	Abcam	Cat#ab8245; RRID: AB_2107448
Goat anti-mouse IgG (H + L), HRP conjugate	Proteintech	Cat#SA00001-1; RRID: AB_2722565
Goat anti-rabbit IgG (H + L), HRP conjugate	Proteintech	Cat#SA00001-2; RRID: AB_2722564
Biological samples		
Human coronary blood samples	Zhongda Hospital affiliated to Southeast University	For patient information, see Table S1
Chemicals, peptides, and recombinant proteins		
DAPI	Sigma	Cat#D9542
Lipofectamine™ 3000	Invitrogen	Cat#L3000001
Phenylmethylsulfonyl fluoride, PMSF	Beyotime Biotechnology	Cat#ST505
Phosphatase inhibitor cocktail	Roche	Cat#M7528
Protease inhibitor cocktail	Thermo Fisher Scientific	Cat#87785
Paraformaldehyde	Sigma Aldrich	Cat#P6148-500G
Fetal Bovine Serum, qualified, heat inactivated	Gibco	Cat#10100147
Dulbecco's modified Eagle's medium (DMEM, high glucose, GlutaMAX™ Supplement)	Gibco	Cat#10566016

(*Continued on next page*)

Continued

REAGENT or RESOURCE	SOURCE	IDENTIFIER
Opti-MEM™ I Reduced Serum Medium, no phenol red	Gibco	Cat#11058021
MG132	MedChemExpress	Cat#HY-13259
Chloroquine	MedChemExpress	Cat#HY-17589A
TRIzol reagent	Invitrogen	Cat#15596026
Critical commercial assays		
Pierce™ Crosslink Magnetic IP/Co-IP Kit	Thermo Fisher Scientific	Cat#88805
Clean-Blot™ IP Detection Kit (HRP)	Thermo Fisher Scientific	Cat#21232
Pierce™ BCA Protein Assay Kit	Thermo Fisher Scientific	Cat#23227
Haematoxylin-Eosin Stain Kit	Solarbio	Cat#G1120; CSTR:19375.09.3101HUMSCSP502
Experimental models: Cell lines		
293T	Chinese Academy of Sciences	Cat#SCSP-502
Experimental models: Organisms/strains		
Mouse: C57BL/6	Laboratory Animal Center of Yangzhou University	N/A
Oligonucleotides		
Acta2 (Mouse) forward: 5′-CATCTTTCATTGGGATGGAGTCAG-3′	This paper	N/A
Acta2 (Mouse) reverse: 5′-CCCCTGACAGGACGTTGTT-3′	This paper	N/A
Col1α1 (Mouse) forward: 5′-GCTCCTCTTAGGGGCCACT-3′	This paper	N/A
Col1α1 (Mouse) reverse: 5′-CCACGTCTCACCATTGGGG-3′	This paper	N/A
Acta2 (Rat) forward: 5′-GTGAAGAGGAAGACAGCACAG-3′	This paper	N/A
Acta2 (Rat) reverse: 5′-ATTCCAACCATCACTCCCTG -3′	This paper	N/A
Col1α1 (Rat) forward: 5′-AGGCATAAAGGGTCATCGTG-3′	This paper	N/A
Col1α1 (Rat) reverse: 5′-ACCGTTGAGTCCATCTTTGC-3′	This paper	N/A
AdshTRIM38	This paper	N/A
AAV9-shRNA-TRIM38	This paper	N/A
Recombinant DNA		
Flag-TRIM38	Liu et al. (2011)	N/A
His-Ubiquitin-K63	Lee et al. (2019)	N/A
HA-TAB2	Criollo et al. (2011); Shi et al. (2008)	N/A
HA-TAB3	Criollo et al. (2011); Shi et al. (2008)	N/A
Myc-TAK1	Kim et al. (2012)	N/A
Software and algorithms		
GraphPad Prism Version 8.0	GraphPad	https://www.graphpad.com/scientificsoftware/prism/; RRID:SCR_002798
IBM SPSS Version 25.0	SPSS	https://www.ibm.com/analytics/spss-statisticssoftware; RRID:SCR_002865
Fiji-ImageJ	National Institute of Health	https://imagej.net/Fiji; RRID:SCR_003070

RESOURCE AVAILABILITY

Lead contact

Further information, requests, and inquiries should be directed to and will be fulfilled by the Lead Contact, Lijuan Chen (chenlijuan@seu.edu.cn).

Materials availability

The study did not generate new unique reagents.

Data and code availability

All data reported in this paper will be shared by the lead contact upon request. This paper does not report original code. Any additional information required to reanalyze the data reported in this paper is available from the lead contact upon request.

EXPERIMENTAL MODEL AND SUBJECT DETAILS

Patient samples

Human blood samples were collected from the coronary arteries of 10 participants undergoing PCI due to undiagnosed chest pain at the Zhongda Hospital affiliated to Southeast University. Diagnosis was based on the "2018 ESC/ACC/AHA/WHF Guidelines for Fourth universal definition of myocardial infarction (2018)"(Thygesen et al., 2018). The exclusion criteria were as follows: previous MI, severe heart failure, advanced liver or renal diseases, chronic or acute infections, autoimmune diseases, abnormal hematopoietic function, and malignancies. The blood samples included those from 5 normal controls and 5 AMI patients (basal clinical characteristics are presented in Tables S1 and S2). Serum was separated at the conditions of 3000 r/min, 30 min, 4°C and stored at −80°C. The expression of TRIM38 in serum was detected by ELISA using human TRIM38 ELISA kit (Thermo Fisher Scientific, China) according to the official operating manual. This study was approved by the Ethics Committee at Zhongda Hospital affiliated to Southeast University. All participants provided written informed consent.

Animal experiments

The animals (8-week-old C57BL/6 male mice; 20−25 g) used in this work were purchased from the Laboratory Animal Center of Yangzhou University (Yangzhou, China), raised under room temperature with a 12-h light/dark cycle, and given free access to food and water. All animal experiments were conducted in accordance with the National Institutes of Health Guide for the Care and Use of Laboratory Animals and approved by the Care of Experimental Animals Committee of Southeast University.

MI models

The mouse MI model was established as previously described (Hao et al., 2020). Briefly, mice were anaesthetised by intraperitoneal injection of 1.5% pentobarbital, and then a volume-controlled small animal respirator was used to support their breathing through a tracheal cannula. Subsequently, a left thoracotomy was performed to expose the heart, and a 6-0 prolene suture on a small, curved needle was passed through the myocardium beneath the left anterior descending (LAD) coronary artery. The root of the LAD coronary artery was permanently ligated to induce myocardial ischemia. Mice in the sham-operated group were subjected to the same surgical procedures, except LAD ligation, and then the chest was closed with 6-0 prolene suture after removing any air. During surgery, the body temperature was maintained at 37°C using a heating pad until the mice recovered completely. Four weeks after surgery, the mice was killed, and the hearts were harvested for further analysis.

Isolation and culture of primary CFs

Primary neonatal CFs were isolated from the heart of Sprague-Dawley (SD) rats (male, 1−3-day-old) and cultured in 75-cm^2 flasks in DMEM/F12 containing 10% foetal bovine serum. In brief, hearts were rapidly removed from anaesthetised infant rats and immediately placed in cold Hanks' Balanced Salt Solution, and the ventricular myocardium was minced into small pieces under sterile conditions. After digestion with 0.125% trypsin for 10 min, the ventricular myocardium was pooled and digested with a mixed enzyme solution containing 0.125% trypsin and 0.08% collagenase type II at 37°C until there was no obvious tissue left. The digested cells in the supernatant were collected and centrifuged at 1000 rpm for 10 min and then pre-plated into cell culture dishes with 10% FBS and incubated with 95% air + 5% CO_2 for 2 h to separate

cardiomyocytes from CFs by adherence. At the end of the differential adhesion process, weakly attached or unattached cells were rinsed free and discarded, the attached CFs were continuously suspended in the cell culture dishes with fresh DMEM/F12 supplemented with 10% FBS for 72 h before any subsequent treatment.

METHOD DETAILS

Adenovirus infection

Rat TRIM38 overexpression and knockdown adenoviruses were purchased from GenePharma (Shanghai, China). Recombinant AdTRIM38 vectors were generated by introducing rat AdTRIM38 cDNA into a replication-defective adenoviral vector. As a control, green fluorescent protein was inserted into the same adenoviral vector. The rat shTRIM38 constructs were ordered from GenePharma (Shanghai, China) to generate AdshTRIM38 adenoviruses. A non-targeting short hairpin RNA (AdshRNA) was used as a control. CFs were infected with different adenovirus in diluted medium at a multiplicity of infection of 100 for 24 h.

Western blot analysis

Whole protein extraction was prepared from CFs using RIPA lysis buffer (Solarbio, Beijing, China) with protease and phosphatase inhibitors. A BCA kit (Thermo, Rockford, IL, USA) was used to measure the protein concentration. Briefly, 50 μg total protein samples were separated by 12% sodium dodecyl sulfate-polyacrylamide gel electrophoresis and transferred to methanol pre-activated polyvinyl difluoride membranes, and then blocked overnight with 10% non-fat milk in Tris-buffered saline at 4°C for 2 h. The membranes were probed with primary antibodies, including TRIM38 (1:200, Cat.MA5-26235; Thermo Fisher Scientific, Shanghai, China), TRIM38 (1:1000, Cat.AF0307; Affinity Biosciences, Jiangsu, China), Collagen I (1:1000, Cat.ab270993; Abcam, Shanghai, China), α-SMA (1:1000, Cat.ab7817; Abcam, Shanghai, China), p-ERK1/2(1:1000, Cat.4370; CST, Shanghai, China), total ERK1/2 (1:1000, Cat.4695; CST, Shanghai, China), p-JNK1/2 (1:1000, Cat.4668; CST, Shanghai, China), total JNK1/2 (1:1000, Cat.9252; CST, Shanghai, China), p-p38 (1:1000, Cat.4511; CST, Shanghai, China), total p38 (1:1000, Cat.9212; CST, Shanghai, China), p-TAK1 (1:1000, Cat.9339; CST, Shanghai, China), p-TAK1 (1:1000, Cat.AF4379; Affinity Biosciences, Jiangsu, China), total TAK1 (1:1000, Cat.4505; CST, Shanghai, China), TAB2 (1:1000, Cat.3745; CST, Shanghai, China), TAB3 (1:600, Cat.sc-166538; Santa, Shanghai, China), HA (1:1000, Cat.3724; CST, Shanghai, China), Myc (1:1000, Cat.2276; CST, Shanghai, China), His (1:1000, Cat.12698; CST, Shanghai, China), Flag (1:1000, Cat.14793; CST, Shanghai, China), and glyceraldehyde 3-phosphate dehydrogenase (GAPDH) (1:1000, Cat.ab8245; Abcam, Shanghai, China) overnight at 4°C with gentle shaking. After washing for three times with Tris-buffered saline containing 0.2% Tween 20 (TBST), membranes were incubated with HRP-conjugated goat anti-mouse (1:5000, Cat.SA00001-1; Proteintech, Wuhan, China) and HRP-conjugated goat anti-rabbit (1:6000, Cat.SA00001-2; Proteintech, Wuhan, China) secondary antibodies for 2 h at room temperature. Subsequently, after development with a chemiluminescent reagent on an ECL imaging system (Tanon-5200, Tanon, Shanghai, China), the protein bands were exposed. Further analysis was carried out using ImageJ software to quantify the protein bands.

Immunofluorescence staining

CFs were cultured on sterile glass and treated with different agents. CFs were washed with PBS once and fixed with 4% formaldehyde in PBS for 15 min at room temperature. The cells were permeabilised with 0.5% Triton X-100 in PBS for 20 min and blocked with 5% goat serum for 1 h at room temperature and then incubated with anti-α-SMA antibody (1:200, Cat.ab7817; Abcam, Shanghai, China) and anti-Collagen I (1:200, Cat.ab270993; Abcam, Shanghai, China) overnight at 4°C. CFs were incubated with the fluorescent secondary antibody in 3% BSA in PBS and counterstained with DAPI for 10 min at room temperature in the dark. The cells were imaged with Nikon Eclipse Ti confocal microscope (Nikon 246, Tokyo, Japan). Green fluorescence was considered a marker of collagen I positivity.

Total RNA isolation and quantitative real-time PCR

TRIzol reagent (Invitrogen) was used to extract total RNA from left ventricular tissues and cultured CFs as described by the manufacturer. RNA was reverse-transcribed into cDNA using the NCode miRNA First-Strand cDNA Synthesis Kit (Invitrogen). Quantitative real-time PCR amplification was performed using the SYBR Green PCR Master Mix (Applied Biosystems). Amplification was performed at 95°C for 10 min, followed by 40 cycles at 95°C for 15 s and 60°C for 1 min. Each PCR was performed in triplicate. GAPDH was used as a reference gene to normalize gene expression, and the $2-\Delta\Delta Ct$ method was utilised to analyse the RT-qPCR data. The

primers used for RT-qPCR were as follows: *Acta2* (Mouse) forward: 5′-CATCTTTCATTGGGATGGAGTCAG-3′ and reverse: 5′-CCCCTGACAGGACGTTGTT-3′; *Col1α1* (Mouse) forward: 5′-GCTCCTCTTAGGGGCCAC T-3′and reverse: 5′-CCACGTCTCACCATTGGGG-3′. *Acta2* (Rat) forward: 5′-GTGAAGAGGAAGACAGCAC AG-3′ and reverse: 5′-ATTCCAACCATCACTCCCTG -3′; *Col1α1* (Rat) forward: 5′-AGGCATAAAGGGTCAT CGTG-3′ and reverse: 5′-ACCGTTGAGTCCATCTTTGC-3′.

Wound healing assay

Wound healing assay was used to evaluate the migratory ability of CFs. In brief, CFs were seeded into 6-well dishes and cultured to confluence. A sterilised 100 μL pipette tip was used to generate a scratch through the diameter, and the debris was washed away. The wound area was captured by an inverted microscope at indicated time points, and then the width of the wound area was evaluated using ImageJ software.

AAV9-mediated gene delivery in the heart

The AAV9-shRNA-TRIM38, AAV9-TRIM38, and virus controls were constructed by GenePharma (Shanghai, China). To obtain an optimal efficacy of cardiac TRIM38 knockdown and overexpression, the AAV9-mediated gene delivery was achieved through intramyocardial injection. Briefly, a 25 μL injection volume containing 5×10^{12} genome particles of virus vectors was injected into three randomly chosen sites within left ventricles. After injection with AAV9 virus vectors for two weeks, an MI operation was conducted. Mice in the sham and MI groups were injected with an equal volume of empty AAV9 vectors.

Histopathology assay

Four weeks after MI surgery, mouse hearts of each group were collected and fixed with 4% formaldehyde for 48 h. The heart tissues were subjected to alcoholic dehydration and embedded in 4% paraffin. The hearts were sliced into 4 μm sections and subjected to HE and Masson's trichrome staining. Areas stained in blue indicate the deposition of collagen fibrils. Thereafter, collagen volume fraction was acquired using Image Pro Plus software to evaluate the degree of myocardial fibrosis. Immunohistochemical staining was performed using anti-collagen I antibody at 37°C for 2 h. After three washes with PBS, the secondary antibody was added. Next, the samples were incubated at 37°C for 2 h and washed with PBS before addition of 3, 3′ diaminobenzidine for 5 min. After haematoxylin counterstaining, dehydration in graded alcohols, and stepping in xylene, neutral gum was used for mounting. Brown granules in the cells were observed using a microscope (Nikon 246, Tokyo, Japan), and five visual fields were randomly selected.

Echocardiography analysis

Mice were anaesthetised with 1.0% inhaled isoflurane and the transthoracic echocardiography was performed with a 250 MHz ultrasound transducer (Vevo 2100, VisualSonics). Then, the LVIDd and the LVIDs were measured. LVEF and LVFS were calculated as follows: LVEF = 100% × stroke volume/end-diastolic volume. LVFS = 100% × (LVIDd–LVIDs)/LVIDd. All measurements were repeated at least three representative cycles and averaged with the same equipment by an experienced technician blinded to the study groups.

Plasmid transfection

Flag-TRIM38 (Liu et al., 2011), His-Ubiquitin-K63 (mammalian expression of His tagged ubiquitin with all lysines mutated to arginines except K63) (Lee et al., 2019), HA-TAB2 (Criollo et al., 2011; Shi et al., 2008), HA-TAB3 (Criollo et al., 2011; Shi et al., 2008), and Myc-TAK1 (Kim et al., 2012) plasmids were purchased from Genechem Biotechnology (Shanghai, China). Plasmid DNA was transfected using LIPOFECTAMINE™ 3000 Transfection Kit (Life Technologies, Carlsbad, CA, USA) according to the manufacturer's protocol.

IP assays

IP was performed as previously described (Chen et al., 2017). Briefly, cultured HEK293T cells were collected and lysed in IP buffer containing 20 mmol/L Tris-HCl (pH 8.0), 150 mmol/L NaCl, 0.5% NP-40, 1 mmol/L EDTA, and a protease inhibitor cocktail. For each IP sample, 500 μL of the cell lysates was incubated with 10 μL protein A/G agarose beads and the indicated antibodies overnight at 4°C. In addition, the matrix was further washed 5–6 times with cold IP buffer, and then 1 × loading buffer was added. The whole-cell lysates and immunoprecipitated proteins were incubated with the indicated primary antibodies. Clean-Blot™ IP Detection Reagent (Cat.21230, Thermo Fisher Scientific, China) was used as the secondary antibody to eliminate detection interference from both the heavy chain (approx. 50 kDa) and the light-chain

(25 kDa) IgG fragments of the antibodies used for the initial immunoprecipitation assay. Each experiment was performed in triplicate.

Ubiquitination assay

The ubiquitination assay was performed as previously described (Chen et al., 2017). Briefly, plasmids coding for flag-tagged protein substrates were co-transfected into HEK293T cells with His-ubiquitin and HA-TAB2, or as indicated. Transfected cells were treated with the proteasome inhibitor MG132 (20 μM, 5 h) before harvesting. HEK293T cells were lysed in SDS lysis buffer containing 20 mmol/L Tris–HCl (pH 7.4), 150 mmol/L NaCl, 1 mmol/L EDTA, 1% SDS, and a protease inhibitor cocktail. Then, the lysates were denatured by heating for 5 min. The supernatants were diluted 10-fold with lysis buffer containing 20 mmol/L Tris–HCl (pH 7.4), 150 mmol/L NaCl, 1 mmol/L EDTA, 1% Triton X-100, and a protease inhibitor cocktail. After centrifugation at 4°C for 10 min, the supernatants were collected and subjected to immunoprecipitation with the indicated antibodies.

QUANTIFICATION AND STATISTICAL ANALYSIS

Continuous values are presented as mean ± standard deviation (SD). The unpaired Student's t-test was used for comparisons between two groups. One-way ANOVA followed by Bonferroni's post-hoc test or Tamhane's T2 post-hoc test was used for comparisons among multiple groups. A two-tailed P-value of <0.05 was considered statistically significant. All statistical analyses were performed using GraphPad Prism Version 8.0 (GraphPad Prism Inc) and IBM SPSS Version 25.0 (SPSS Inc).